

Application of the One-Dimensional Turbulence model to incompressible channel and pipe flow

Juan A. Medina M. · Heiko Schmidt · David. O. Lignell

Received: date / Accepted: date

Abstract Incompressible channel and pipe flow configurations are investigated using the One-Dimensional Turbulence (ODT) model, in which the 1-D domain is aligned with the wall normal direction. The framework for the application of ODT in planar and cylindrical coordinates is revisited for the temporal ODT channel and pipe flow configurations and a new spatial formulation is introduced. The calculation of the turbulent kinetic energy (TKE) budgets in ODT for the temporal and spatial formulations is reviewed for the planar channel flow and newly introduced in cylindrical pipe flow. Simulations are performed at three different friction Reynolds numbers, 550, 1000 and 2000 in order to compare ODT results in the planar and cylindrical formulation with Direct Numerical Simulations (DNS) from Chin et al. [Int. J. Heat Fluid Flow 45 (2014) 33-40] and Khoury et al. [Flow, Turbul. Comb. 91 (2013) 475-495]. ODT results are generated for both the temporal and spatial formulations for the normalized mean velocity profiles, streamwise RMS velocity profiles, wall normal Reynolds stress component, TKE production and dissipation budgets, and the pre-multiplied mean velocity gradient. DNS results are generally captured very well by ODT. This shows that ODT is a reduced order model that is able to capture a significant part of the flow dynamics in wall-bounded flows.

Keywords ODT · channel · pipe · temporal · spatial

1 Introduction

Although the canonical channel and pipe flow configurations have been studied extensively, there are still numerous issues in the field of wall-bounded flows that have not been properly addressed. A very detailed list of issues and the current state of the art is presented by Marusic et al. [19]. Open discussions in wall-bounded flows focus on the structure and scaling of wall turbulence at high Reynolds numbers. On one hand, there is the classical scaling research, directly related to the mean velocity behavior and the two principal regions of the velocity profile that follow distinct scalings. On the other hand, there is the more complex topic of observation of coherent organized motions and their effect on turbulent interactions, e.g. in the turbulence production [19].

A comprehensive study on the mean velocity characteristics in turbulent pipe flow is given by Wu and Moin [29]. This study presents a solid discussion from the classical scaling point of view by means of Direct Numerical Simulations (DNS), for a range of bulk Reynolds numbers $5300 < Re_D < 44000$. Monty et al. [22] provides a detailed introduction and experimental results of the large-scale structures away from the wall, and how they are more likely to grow at a greater rate with distance from the wall in channels. Also adding to this point is the discussion presented by Kim and Adrian [13], regarding the existence of very large-scale motions (VLSMs), prominent in the logarithmic layer of turbulent pipe flow. The VLSMs become increasingly energetically dominant as the Reynolds number increases.

Significant contributions that could help elucidate the open questions in wall-bounded flows could and should be eventually addressed by DNS. However, DNS have pushed the limits of current computational power, yet only modest Reynolds numbers up to $Re_\tau = 2003$ have been achieved for pipe flow [2]. The simplicity of the

J. A. Medina M., H. Schmidt
BTU Cottbus-Senftenberg, Siemens-Halske-Ring 14, 03046 Cottbus, Germany
Tel.: +49(0)-355-69-4813
E-mail: medinjua@b-tu.de

D. O. Lignell
Brigham Young University, 350, Clyde Building, UT-84602 Provo, USA.

channel flow configuration allowed the achievement of these moderately high Reynolds numbers earlier [6, 15]. There is an important lag between DNS studies and experimental turbulence measurements, given that the latest experimental studies have been able to achieve Re_τ up to 98000 [7].

In order to overcome the gap between physically realistic Reynolds numbers and the capabilities of current DNS, a reduced order stochastic model was developed by A. Kerstein, the One-Dimensional Turbulence (ODT) model [10]. As a reduced order model, ODT does not solve the generalized Navier-Stokes equations, but instead models 3-D turbulence by means of a solution dependent sequence of stochastic 1-D eddy events. So far, the ODT model has been validated in a variety of flows (see e.g. [9, 11, 14, 17, 20, 21, 26]). In this study, we focus on the cylindrical formulation for incompressible pipe flow in ODT, as a way to extend the model into more complex flows. The cylindrical formulation for ODT was first introduced in [14].

In this paper, Section 2 provides the model and implementation details for the simulation of incompressible channel and pipe flow. We begin with a very detailed explanation of the derivation of the diffusion equations in ODT for the temporal formulation and we then generalize and expand some concepts for a new spatial formulation for closed lines in Section 2.1. Afterwards, in Section 2.2, we review details regarding the implementation of the turbulent advection in ODT, relying heavily on the work of [18] for general aspects of the cylindrical formulation, and focusing the analysis on the limitations encountered by the general cylindrical formulation in closed lines. Section 3 details the derivation of relevant statistical quantities in ODT, with the purpose of deriving and introducing the cylindrical ODT turbulent kinetic energy (TKE) equation. Section 4 explains the problem setup and presents ODT results compared to DNS data from [2, 6, 8, 12, 15, 23]. The results comprise the evaluation of mean velocity profiles, RMS velocity profiles, budgets for TKE production and dissipation, Reynolds stresses and pre-multiplied energy spectra for a set of Reynolds numbers $Re_\tau \approx 550, 1000, 2000$. Finally, some concluding remarks are provided in Section 5.

2 ODT model formulation for incompressible channel and pipe flow

In the ODT model, the deterministic solution of 1-D diffusion (and/or reaction) evolution equations is coupled to the stochastic implementation of 1-D eddy events. An eddy event in ODT models the effects of turbulent transport due to eddies on the 1-D property profiles of the flow. Concurrently, the deterministic diffusion process catches up to implemented eddy events, in what could be considered as a two-step operator splitting approach. Following this categorization, the form and derivation of the 1-D deterministic diffusion equations is described next in Section 2.1, while details of the eddy event implementation are given afterwards in Section 2.2.

2.1 Deterministic momentum diffusion and enforcement of mass and energy conservation

2.1.1 Temporal ODT Formulation

Formulations in this work are based on a Lagrangian framework, as in [17]. The planar (or Cartesian) form of the equations for momentum diffusion is derived in [17]. Therefore, we focus on the derivation for the cylindrical form of the equations. The reader is encouraged to consult the work of Sutherland et al. [28] for a detailed derivation of several planar ODT formulations up to this date. Before proceeding to the derivation of the diffusion equations, we stress that all of the expressions used here related to conservation of mass, momentum and energy, refer to the conservation of these quantities considering only linear effects during the deterministic diffusion advancement. During an eddy event, these quantities are satisfied by construction, as we will detail later

The temporal ODT formulation (T-ODT) for pipe flow can be visualized as a fixed ODT line in the radial direction of a pipe. The temporally developing flow across the line is simulated in this formulation. Application of the Reynolds Transport Theorem (RTT) allows the derivation of the diffusion equations [28],

$$\begin{aligned} \frac{d}{dt} \int_{\mathcal{V}_\Psi} \rho \Psi d\mathcal{V} &= \int_{\mathcal{V}} \frac{\partial (\rho \Psi)}{\partial t} d\mathcal{V} + \oint_S (\rho \Psi \circ \mathbf{V}_S) \cdot \mathbf{n} dS + \oint_S [\rho \Psi \circ (\mathbf{V}_\Psi - \mathbf{V}_S)] \cdot \mathbf{n} dS, \\ \frac{d}{dt} \int_{\mathcal{V}_\Psi} \rho \Psi d\mathcal{V} &= \frac{d}{dt} \int_{\Omega} \rho \Psi d\Omega + \oint_S [\rho \Psi \circ (\mathbf{V}_\Psi - \mathbf{V}_S)] \cdot \mathbf{n} dS. \end{aligned} \quad (1)$$

Eq. (1) is the generalized RTT for a vector of intensive field quantities Ψ and ρ is the corresponding density. Eq. (1) can be directly associated to momentum conservation whenever Ψ is substituted by a velocity field. The standard dyadic product \circ is used here. The first line of the equation is the relation between a Lagrangian system of volume \mathcal{V}_Ψ and an Eulerian system \mathcal{V} with boundary S and unitary normal vector \mathbf{n} . $\mathbf{V}_\Psi = [u_\Psi, v_\Psi, w_\Psi]^T$ refers to the boundary velocity of the Lagrangian system \mathcal{V}_Ψ , while \mathbf{V}_S is the boundary velocity of the Eulerian system

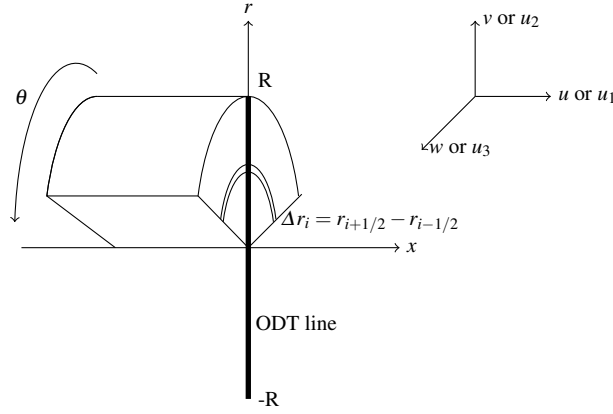


Fig. 1: Representation of an ODT line in a cylindrical coordinate system. An exemplary cell with size Δr_i is shown to illustrate the form of the effective area/volume element of the cell, i.e. a ring element.

\forall . The second line of the equation is a relation between equivalent Lagrangian systems \forall_{Ψ} and Ω . We write explicitly the Eulerian and Lagrangian equivalences of the RTT, given that they will be useful to illustrate the notion of open and closed systems in the ODT diffusion evolution. The evolution of $\rho\Psi$ is also given by the net diffusive flux $\underline{\Phi}_{\Psi}$ across S ,

$$\frac{d}{dt} \int_{\forall_{\Psi}} \rho\Psi d\forall = \oint_S \underline{\Phi}_{\Psi} \cdot \mathbf{n} dS. \quad (2)$$

We now formulate a 1-D Lagrangian approach, in which the boundary velocity $\mathbf{V}_S = [0, v_s, 0]^T$ equates the mass-averaged velocity $\mathbf{V}_D = [u_D, v_D, w_D]^T$ at the boundaries along the line direction, $v_s = v_D$. The subindex D is used here to indicate that the Lagrangian volume deforms in order to guarantee no incoming or outgoing fluxes with respect to the mass-averaged velocity and v is in this case the velocity component aligned in the line direction. The convention follows the coordinate system in Figure 1. Due to the single phase and non-reactive nature of the system, $\mathbf{V}_D = \mathbf{V}_{\Psi}$. Since the formulation is merely 1-D, this implies that the term $\oint_S [\rho\Psi \circ (\mathbf{V}_{\Psi} - \mathbf{V}_S)] \cdot \mathbf{n} dS = 0$. For momentum conservation, transporting a quantity $\Psi = \mathbf{V}$ in Eq. (1) and using Eq. (2) with $\underline{\Phi}_{\Psi} = -p\underline{\mathbf{1}} + \underline{\underline{\tau}}$, we obtain,

$$\frac{d}{dt} \int_{\Omega} \rho\mathbf{V} d\forall = - \int_{\forall} (\nabla \cdot p\underline{\mathbf{1}}) d\forall + \int_{\forall} (\nabla \cdot \underline{\underline{\tau}}) d\forall. \quad (3)$$

In obtaining Eq. (3), the Divergence Theorem was applied to substitute the surface integral terms from Eq. (1) with the corresponding volume integral terms. p is the hydrodynamic pressure, $\underline{\underline{\tau}}$ is the shear stress tensor and $\underline{\mathbf{1}}$ is the identity matrix.

The coordinate system from Fig. 1 is modified in such a way that we can work with both positive and negative values of r . The swept angle for a given cylindrical section is arbitrary. In general, we are interested in cells along the line that construct the shape of a cylindrical ring whenever a certain swept angle $\Delta\theta$ and some shell thickness Δx is assumed. Generally speaking, the volume differential element for any cylindrical sector resembling the one shown in Figure 1 is $d\forall = r dr \Delta x \Delta\theta$.

We now consider streamwise momentum conservation for simplicity, i.e. the scalar version of Eq. (3) for the u component of \mathbf{V} . For the streamwise direction, the equivalent shear stress divergence in Eq. (3) takes the form $(1/r)[\partial(r\tau_{rx})/\partial r] + (1/r)(\partial\tau_{\theta x}/\partial\theta) + \partial\tau_{xx}/\partial x$. In the one-dimensional formulations used with ODT, we neglect the last two terms in the previous expression. The reader should note that $\tau_{rx} = \mu\partial u/\partial r$, whereby μ is the dynamic viscosity. For the pressure gradient, the applicable term is $\partial p/\partial x$, which can be decomposed into mean and fluctuating components, $\partial\bar{p}/\partial x$ and $\partial p'/\partial x$. The mean component is constant for incompressible channel or pipe-flow (in our case, a Fixed Pressure Gradient forcing, FPG). The effect of the fluctuating component can be ignored during the diffusion evolution, since it is part of the turbulent transport modeling explained later. These considerations lead to,

$$\frac{d}{dt} \int \rho u r dr = - \int \frac{\partial\bar{p}}{\partial x} r dr + \int \frac{1}{r} \frac{\partial}{\partial r} \left(r \mu \frac{\partial u}{\partial r} \right) r dr. \quad (4)$$

Eq. (4) is discretized by means of a Finite Volume Method (FVM). Details of the discretization and numerical method are given in Appendix A. We note that Eq. (4) might encounter an apparent singularity at $r = 0$. We avoid this singularity by using a symmetric center cell with fixed size, and solving a flux equalization condition

for this cell (see Appendix A for details). For simultaneous enforcement of mass and energy conservation in the zero Mach number limit, the divergence condition of the velocity field must be enforced as in [20]. We note that, for closed systems, the second term on the RHS of Eq. (1) is $\oint_S (\rho \Psi \circ \mathbf{V}_S) \cdot \mathbf{n} dS = 0$, whenever the integral over the whole domain is evaluated. This is due to the 1-D formulation and the boundary velocities $v_{\text{Boundary}} = 0$. A similar reasoning would apply for periodic Boundary Conditions. Cell-wise, this term can be decomposed into a linear and a non-linear flux term by \mathbf{V}_S . The latter is neglected during diffusion evolution. We can then deduce that $d/dt(\int_{\Omega} \rho \Psi d\mathcal{V}) = \int_{\mathcal{X}} [\partial(\rho \Psi)/\partial t] d\mathcal{V}$ holds, as long as we enforce $\oint_S [\rho \Psi \circ (\mathbf{V}_{\Psi} - \mathbf{V}_S)] \cdot \mathbf{n} dS = 0$ in Eq. (1). In 1-D, this is essentially the same as displacing the cell interfaces with the velocity v_D , whereby v_D is given by a 1-D divergence condition [20],

$$v_D = \frac{dr}{dt}, \quad \text{with} \quad \frac{1}{r} \frac{\partial}{\partial r} (rv_D) = S_{Div}. \quad (5)$$

In Eq. (5), v_D is the velocity component along the line direction defined at the cell interfaces and S_{Div} is the divergence condition. We have written the divergence condition in differential form for ease of understanding and to stress that it must be applied locally at each cell, in order to ensure local and global enforcement of $\oint_S [\rho \Psi \circ (\mathbf{V}_{\Psi} - \mathbf{V}_S)] \cdot \mathbf{n} dS = 0$ in Eq. (1). We do stress, however, that this condition can also be written in integral terms by use of the divergence theorem. For incompressible flow, $\nabla \cdot \mathbf{V}_D = S_{Div} = 0$, and therefore no cell-interface displacement is required. This conclusion is equivalent to the fact that solving for continuity is trivial in this case, since with $\Psi = 1$ and the vector $\Phi_{\Psi} = \mathbf{0}$ in the scalar version of Eq. (2),

$$\frac{d}{dt} \int_{\Omega} \rho d\mathcal{V} = 0. \quad (6)$$

Eq. (6) is trivially satisfied given that neither Ω nor ρ are time-dependent functions. A word of caution is given here, in the sense that Eq. (5) should be used ideally for closed systems (closed lines) only. When solving open lines, the term $\oint_S (\rho \Psi \circ \mathbf{V}_S) \cdot \mathbf{n} dS$ is not necessarily 0, given that the boundary velocities may not be of the same magnitude. Therefore, continuity is solved in these cases by means of a first-order approximation in time (or in space), as it has been done traditionally in ODT formulations (see [17, 18, 28] for details).

With the before mentioned considerations, the discretization and solution of Eq. (4) with a FVM is straightforward. For the purpose of completion, we repeat the resulting expression for streamwise momentum conservation in the planar case (channel flow), for an ODT line coinciding with the wall-normal direction y . This expression was already derived in [17],

$$\int \frac{\partial(\rho u)}{\partial t} dy = - \int \frac{\partial \bar{p}}{\partial x} dy + \int \frac{\partial}{\partial y} \left(\mu \frac{\partial u}{\partial y} \right) dy. \quad (7)$$

We note that for the v and w velocity components in the planar case, the resulting expressions are essentially the same as Eq. (7), except for the pressure gradient term that is ignored (see [17]). For the cylindrical case, however, we do not derive expressions for v and w due to theoretical considerations (see Section 3.2.1).

2.1.2 Spatial ODT Formulation

The spatial ODT formulation (S-ODT) is a 2-D approximation of a quasi-stationary flow. In S-ODT, the ODT line moves along the streamwise direction in order to reconstruct a static 2-D picture of the flow. For this purpose, the terms including time derivatives d/dt are neglected in Eq. (1). For momentum conservation, using the divergence theorem to replace the surface integrals in Eq. (1-2), and considering $\Psi = \mathbf{V}$ and $\Phi_{\Psi} = -p\mathbf{1} + \underline{\underline{\tau}}$, we obtain

$$\int_{\mathcal{X}} \nabla \cdot [\rho \mathbf{V} \circ (\mathbf{V}_{\Psi} - \mathbf{V}_S)] d\mathcal{V} = - \int_{\mathcal{X}} (\nabla \cdot p\mathbf{1}) d\mathcal{V} + \int_{\mathcal{X}} (\nabla \cdot \underline{\underline{\tau}}) d\mathcal{V}. \quad (8)$$

We stress that for this 2-D approach, we have $\oint_S (\rho \Psi \circ \mathbf{V}_S) \cdot \mathbf{n} dS = 0$ along the whole domain in Eq. (1). This is due to the zero boundary velocity in the line direction and the zero velocity of the Eulerian boundary overall in any direction perpendicular to the line, given the effective zero thickness of our reference frame. Now consider again the cylindrical coordinate system from Figure 1. The ODT line is oriented in radial direction and is assumed to move downstream in the axial direction x . Since there are two spatial dimensions readily available for the formulation (r and x), the volume/area differential element is $d\mathcal{V} = r dr dx \Delta \theta$. Due to the 2-D formulation, there is a possibility to choose the shear stress divergence as $(1/r)[\partial(r\tau_{rx})/\partial r] + \partial\tau_{xx}/\partial x$ for the u velocity component. Although this is theoretically consistent, preserving both the radial and axial terms in the shear stress results into an elliptic PDE. This is not solvable as a spatially marching problem, and it is also not clear how this would affect the instantaneous eddy event implementation. This is one of the main limitations of

the S-ODT formulation, as detailed in [1]. For this reason, the axial shear stress gradient is neglected in the spatial formulation. A similar reasoning forbids the use of a variable axial pressure gradient $\partial p/\partial x$. At most, a constant forcing FPG $\partial \bar{p}/\partial x$ can be imposed, as in the T-ODT formulation.

Due to the 2-D approach we must generalize now $\mathbf{V}_\Psi - \mathbf{V}_S$ to $\mathbf{V}_\Psi - \mathbf{V}_S = [u_D, 0, w_D]^T$ in Eq. (8). This is because we can ensure at most that $\mathbf{V}_\Psi = [u_D, v_D, w_D]^T$ and $\mathbf{V}_S = [0, dr/dt = v_S = v_D, 0]^T$. These considerations lead to the following expression for the streamwise momentum conservation,

$$\iint \frac{\partial(\rho u u_D)}{\partial x} r dr dx = - \iint \frac{\partial \bar{p}}{\partial x} r dr dx + \iint \frac{1}{r} \frac{\partial}{\partial r} \left(r \mu \frac{\partial u}{\partial r} \right) r dr dx. \quad (9)$$

The final expression is obtained after differentiating Eq. (9) with respect to x due to the effectively infinitesimal character of the line in the x direction. This is also the reason to assume $u_D = u$, the mass-averaged velocity in streamwise direction,

$$\int \frac{\partial(\rho u^2)}{\partial x} r dr = - \int \frac{\partial \bar{p}}{\partial x} r dr + \int \frac{1}{r} \frac{\partial}{\partial r} \left(r \mu \frac{\partial u}{\partial r} \right) r dr. \quad (10)$$

The numerical method used to solve Eq. (10) is detailed in Appendix A. We note that a solution for Eq. (10), might involve positive and negative roots for the streamwise velocity u . However, each velocity component should evolve independently during diffusion and due to the application of the FPG, strictly positive velocity profiles will remain positive, thus allowing the consistency with the spatial marching solution approach.

As in the temporal formulation, simultaneous enforcement of mass and energy conservation is given by the divergence condition in the zero Mach limit. However, this is again another limitation in our spatial formulation for a pipe flow, since the divergence condition for a 2-D flow mandates $\partial u_D/\partial x + (1/r)[\partial(rv_D)/\partial r] = S_{Div}$. Since $\mathbf{V}_S = [0, dr/dt = v_D, 0]^T$, we cannot enforce $\partial u_D/\partial x$ in the 2-D divergence condition by displacing the cell interfaces in streamwise direction x (the line is effectively infinitesimal in x). Thus, in order to find an expression for $\partial u_D/\partial x$ that can be substituted in the divergence condition, an elliptic operator such as the pressure in the streamwise momentum equation must be applied. Since we required a constant axial pressure gradient, we can expect that $\partial u_D/\partial x$ in the divergence condition will only be satisfied in the forced fully developed regime, when $u_D = u$. Therefore, we cannot consider the 2-D divergence condition due to its relation with the elliptic character of the flow. We return then to the 1-D divergence condition for v_D at the cell interfaces, but we use $v_D = dr/dt = u dr/dx$, in order to relate the time t with the spatial advancement x ,

$$v_D = u \frac{dr}{dx}, \quad \text{with} \quad \frac{1}{r} \frac{\partial}{\partial r} (rv_D) = S_{Div}. \quad (11)$$

As in the temporal formulation, this condition is trivially satisfied for $S_{Div} = 0$. Once again, we remark that all of these considerations are only valid for closed lines as in the case of a pipe flow, where the boundary conditions at the wall mandate $\oint_S (\rho \Psi \circ \mathbf{V}_S) \cdot \mathbf{n} dS = 0$ in Eq. (1). Otherwise, continuity can be solved directly by means of a first-order approximation in space (see [17, 18] for details).

For completion, we now show the resulting momentum conservation for the spatial formulation in the planar case (channel flow), already derived in [17],

$$\int \frac{\partial(\rho u^2)}{\partial x} dy = - \int \frac{\partial \bar{p}}{\partial x} dy + \int \frac{\partial}{\partial y} \left(\mu \frac{\partial u}{\partial y} \right) dy. \quad (12)$$

We do not examine the resulting terms for the v and w velocity components in the planar case, since the spatial triplet map formulation forbids the use of more than one velocity component for the channel and pipe-flow cases (see Section 2.2.2).

2.2 Stochastic turbulent advection

The stochastic turbulent advection process in ODT has been extensively detailed in previous ODT publications. In this work, we focus on the implementation of eddy events in a cylindrical coordinate system. This was introduced by Krishnamoorthy [14] and recently presented in a more general framework by Lignell et al [18].

As in previous ODT implementations, there are three main parameters governing the implementation of an eddy event, also known as a triplet map transformation: y_0 , l and λ . y_0 refers to the eddy position, specifically the position of the left edge of the eddy; l is the eddy size; λ is an eddy rate distribution governing the sampling and selection of eddies, which will be detailed later in Section 2.2.3. Operationally, the triplet map is defined as a threefold spatial reduction or compression of a given property profile within some specific eddy range l . This compressed profile is then copied three times along the eddy range with the middle copy spatially inverted. This procedure conserves all quantities within the eddy range and introduces no discontinuities in the function. Only the cylindrical triplet map formulation is presented in this work. For details regarding the planar formulation, we refer to Kerstein [10].

2.2.1 Cylindrical Triplet Map

Based on physical reasoning, the cylindrical triplet map formulation is stated for $r \in \mathbb{R}$ instead of the traditional cylindrical treatment of $r \in \mathbb{R}^+$ (non-negative real numbers including 0). This treatment of the cylindrical system allows the occurrence of eddy events involving the centerline, i.e. eddies are allowed to cross the centerline, as in any physical flow.

Since the line integral in a cylindrical system is defined with a differential element rdr , we opt to conserve an effective surface in the cylindrical formulation of the triplet map. The effects of the stochastic eddy events, implemented as triplet maps, which involve wrinkling of the properties profiles in the radial direction, can be seen as an assumption that holds for fully developed pipe flows and which is consistent with the 1-D implementation. However, this assumption does not necessarily generalize for other types of cylindrical flows, e.g. in helical flows, where the dominant motion is occurring along the tangential direction. In such cases, modifications of the triplet map and diffusion evolution equations would be necessary. Different formulations for the cylindrical triplet map are also possible, in contrast to the more standardised planar triplet map formulation. Lignell et al. [18] introduces several formulations for the triplet map, among which the so-called Triplet Map A (TMA) formulation is the easiest one to understand, given its direct analogy to the planar case. In this work, we make use of the TMA formulation.

The surface, or volume of the eddy \mathbb{V}_{eddy} for the cylindrical formulation, can be expressed as

$$\mathbb{V}_{eddy} = \Delta\theta \left[\int_0^{r_0+l} rdr - \int_0^{r_0} rdr \right]. \quad (13)$$

This equation has been formulated considering that $r_0 \geq 0$ for simplicity and it is equivalent to the volume integral $\Delta\theta \int_{r_0}^{r_0+l} rdr$.

As in the planar case, the threefold compression of the original profile results in the effective volume of an eddy segment, here denoted as $\mathbb{V}_{l/3}$,

$$\mathbb{V}_{l/3} = \frac{\Delta\theta}{3} \left[\int_0^{r_0+l} rdr - \int_0^{r_0} rdr \right]. \quad (14)$$

Each segment is defined within two internal boundaries. The position of each one of the four boundaries can be expressed with the notation r_m with $m \in \{1, 2, 3\}$ and $r_0 = r_{m-1}$ for $m = 1$. Each one of the three compressed segments accounts then for an effective volume,

$$\mathbb{V}_{l/3} = \Delta\theta \left[\int_0^{r_m} rdr - \int_0^{r_{m-1}} rdr \right]. \quad (15)$$

With this notation, the first boundary is r_0 and the last boundary is $r_3 = r_0 + l$. Thus, equating Eq. (14) with Eq. (15) and solving for the internal boundary r_m results in,

$$r_m = \left\{ \frac{1}{3} [(r_0 + l)^2 - r_0^2] + r_{m-1}^2 \right\}^{\frac{1}{2}}. \quad (16)$$

Algorithmically, this implies that the calculation of a boundary r_m is done based on the data from the previous boundary r_{m-1} .

We now generalize Eq. (15) for the case when r_0 is either positive or negative. For that, we make use of the sgn (signum) and modulus functions,

$$\mathbb{V}_{l/3} = \Delta\theta \left[\int_0^{|r_m|} rdr - \text{sgn}(r_m) \text{sgn}(r_{m-1}) \int_0^{|r_{m-1}|} rdr \right]. \quad (17)$$

In Eq. (17), the volume can be positive or negative. The latter occurs when r_m and r_{m-1} have both negative sign. A similar procedure can be used to generalize Eq. (16),

$$|r_m| = \left\{ \frac{1}{3} [(r_0 + l)^2 - \text{sgn}(r_0 + l) \text{sgn}(r_0) r_0^2] + \text{sgn}(r_m) \text{sgn}(r_{m-1}) r_{m-1}^2 \right\}^{\frac{1}{2}}. \quad (18)$$

Eq. (18) is implicit due to the presence of the $\text{sgn}(r_m)$ term and the LHS modulus. Only one of the two possible solutions is real and within the range $[r_0, r_0 + l]$ in this case.

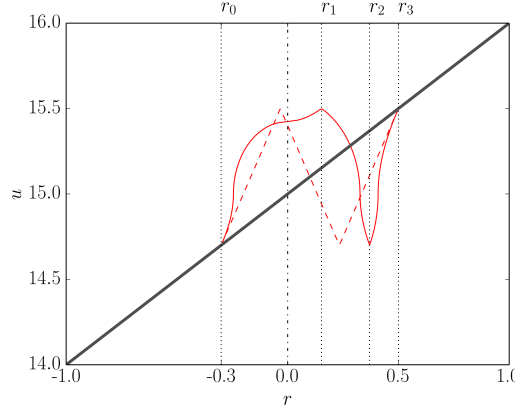


Fig. 2: Application of a cylindrical triplet map in the range $[-0.3, 0.5]$ to a scalar velocity profile $u(r)$. The figure shows the original profile (thick line) and the mapped profile. The internal boundaries r_m from each of the three segments of the triplet map are also shown (dotted lines), as well as the axis line ($r = 0$) (dash-dot line). For comparison, the planar triplet map for the same interval has been drawn with dashed lines.

In order to determine the general expressions for the mapping function of a position $f(r)$ into a new position r , we apply a similar procedure to that used to obtain Eq. (14, 17) and (18). The effective volume of an eddy segment extending from the boundary r_0 to an original position $f(r)$ is conserved and compressed to $1/3$ of its magnitude,

$$\mathbb{V}_{f(r)} = \frac{\Delta\theta}{3} \left[\int_0^{|f(r)|} r dr - \text{sgn}[f(r)] \text{sgn}(r_0) \int_0^{|r_0|} r dr \right]. \quad (19)$$

And conversely, for any mapped position r , that is referenced to the internal boundary r_{m-1} , the effective volume is,

$$\mathbb{V}_r = \Delta\theta \left[\int_0^{|r|} r' dr' - \text{sgn}(r) \text{sgn}(r_{m-1}) \int_0^{|r_{m-1}|} r' dr' \right]. \quad (20)$$

Eq. (19) and (20) can be equated, given that any position $f(r)$ will be mapped to a position r within any of the intervals $[r_{m-1}, r_m]$ for $m \in \{1, 2, 3\}$. This leads to the formal triplet map formulation in a cylindrical coordinate system, as illustrated by Fig. 2, where the middle segment changes the sign of the slope as in the planar definition,

$$f(r) = \begin{cases} \text{sgn}[f(r)] \left\{ \text{sgn}[f(r)] \text{sgn}(r_0) r_0^2 + 3 [r^2 - \text{sgn}(r) \text{sgn}(r_0) r_0^2] \right\}^{1/2} & r_0 \leq r \leq r_1, \\ \text{sgn}[f(r)] \left\{ \text{sgn}[f(r)] \text{sgn}(r_0) r_0^2 - 3 [r^2 - \text{sgn}(r) \text{sgn}(r_1) r_1^2] \right\}^{1/2} & r_1 \leq r \leq r_2, \\ \text{sgn}[f(r)] \left\{ \text{sgn}[f(r)] \text{sgn}(r_0) r_0^2 + 3 [r^2 - \text{sgn}(r) \text{sgn}(r_2) r_2^2] \right\}^{1/2} & r_2 \leq r \leq r_0 + l. \end{cases} \quad (21)$$

We note the nonlinear post-triplet map profiles that occur in cylindrical coordinates, as seen in Figure 2. This is a consequence of the geometric stretching and it is discussed at length in the work of Lignell et al [18].

2.2.2 Kernel function and ODT model parameter α

ODT can be used with a single velocity component, or in a vector formulation, in which three velocity components are modeled. The latter is facilitated with a so-called kernel function that is added to velocity components after mapping to effect inter-component energy transfer in a way that conserves both momentum and energy. In the case of the single velocity component treatment, the measure preserving property of the triplet map guarantees kinetic energy conservation [10], given that the line integral of u^2 would be conserved before and after mapping. Generally, however, it is desired to model the 3-D dynamics with ODT, and therefore many studies rely on the implementation of the previously mentioned kernel function [9, 17, 20]. The kernel implementation is reviewed in detail in [1] for the temporal and spatial planar formulations of ODT and it will not be discussed here. In general, for the planar ODT formulation, the velocity mapping in ODT follows the vector formulation [1],

$$u_k(y) \rightarrow u_k[f(y)] + c_k K(y) + b_k J(y). \quad (22)$$

Here, $K(y), J(y)$ are kernel functions, while c_k and b_k are the respective kernel function coefficients, as defined in [1] for the planar ODT formulation. We switch the notation in this section to u_k for the velocity components

($k \in \{1, 2, 3\}$). $J(y)$ is a second kernel, which is written here only for the purpose of completeness, since it is only needed for variable density flows [1]. $f(y)$ is the triplet map transformation defined in [10].

In the case of pipe flows, the planar philosophy is maintained concerning the application of two kernel functions to the mapped velocity field, as in Eq. (22), but substituting y by r . Also, $f(y)$ is changed to $f(r)$, whereby $f(r)$ refers to the transformation rule given in the cylindrical case by Eq. (21). As in the planar case, the kernel functions K, J are defined as

$$K(r) = r - f(r), \quad J(r) = |K(r)|. \quad (23)$$

A detailed procedure and all of the equations for the calculation of the Kernel functions in the cylindrical formulation can be found in the work done by Krishnamoorthy [14] (set of equations 4.14-4.44) and Lignell et al [18]. We do not discuss the Kernel implementation in this work. Rather, we focus on the influence of an important model parameter in ODT, α , that governs the available energy redistribution between velocity components during the triplet map implementation.

We note that momentum conservation before and after the eddy event in the T-ODT formulation implies

$$\int_{r_0}^{r_0+l} \rho[f(r)] \{u_k[f(r)] + c_k K(r) + b_k J(r)\} r dr = \int_{r_0}^{r_0+l} \rho[f(r)] u_k[f(r)] r dr. \quad (24)$$

The reader should note that, strictly speaking, the RHS of Eq. (24) shows the mapped profiles $\rho[f(r)]$ and $u_k[f(r)]$ instead of the original profiles $\rho(r)$ and $u_k(r)$, due to the necessary condition for mass conservation in the line during an eddy event. Mass conservation is obtained by the measure preserving property of the triplet map transformation while mapping the density $\int \rho(r) r dr = \int \rho[f(r)] r dr$. Since the transformation rule is applied simultaneously to all of the flow variables, the starting point for the discussion of the kernel functions effects in the energy exchange procedure must consider the already mapped scalar profiles.

For the spatial formulation S-ODT in cylindrical pipe flow, the resulting momentum conservation gives

$$\int_{r_0}^{r_0+l} \rho[f(r)] u_1[f(r)] \{u_k[f(r)] + c_k K(r) + b_k J(r)\} r dr = \int_{r_0}^{r_0+l} \rho[f(r)] u_1[f(r)] u_k[f(r)] r dr. \quad (25)$$

The appearance of u_1 arises from the net streamwise momentum flux in the spatial formulation (the line is advected with velocity $u = u_1$ in index notation). Generally speaking, all of the equations that are valid for temporal flow, are also applicable to the spatial formulation, by considering the multiplication by the additional factor $u_1[f(r)]$, which is the mapped streamwise advecting velocity responsible for the flux in the spatial formulation (refer to [14] for details). As explained in [14] for pipe flow, and in [1] for planar flow, Eq. (25) is not internally consistent, since the factor $u_1[f(r)]$ is multiplied both in the LHS (after triplet mapping) and RHS (before triplet mapping). Instead of the fully mapped and kernel-transformed function on the LHS, only the mapped function appears. This is normally not a problem, since the traditional spatial formulation considers one additional step for the eddy implementation, in which the discretized cell boundaries are moved to new lateral locations in order to conserve streamwise fluxes [1]. That is, a coordinate transformation $r \rightarrow \hat{r}$ takes place after mapping, such that

$$\int_{\mathbf{x}} \{u_1[f(r)] + c_1 K(r) + b_1 J(r)\} \hat{r} d\hat{r} = \int_{\mathbf{x}} u_1[f(r)] r dr. \quad (26)$$

Eq. (26) is the solution for streamwise momentum conservation based on lateral displacements. Integrals in Eq. (26) are solved on a cell-wise basis with a FVM, thus allowing the calculation for the new coordinates \hat{r} , which allow consistency of Eq. (25). An important limitation arises in the spatial formulation at this point. For wall-bounded flows such as the channel and pipe flow problems discussed here, there cannot be any cell displacement at the domain boundaries. Since Eq. (26) cannot be used, Eq. (25) is inherently non-conservative in a variable density spatial formulation that involves closed lines. Alternatives could be considered, e.g. by performing a similar treatment to the divergence enforcement in the diffusion step explained in Section 2.1.2. For constant density, however, it is still possible to force consistency of Eq. (25) if both b_k and c_k are 0. This is achieved by setting the ODT model parameter $\alpha = 0$ (refer to the equations in [1] for details). By doing this, the measure preserving property of the triplet map transformation ensures conservation of streamwise momentum flux. The latter is the approach followed in this work for the S-ODT formulation.

2.2.3 Eddy event implementation

The implementation of an eddy event in ODT is governed by a sampling process based on the rate distribution $\lambda(r_0, l, t)$ (or $\lambda(r_0, l, x)$ in the spatial formulation). For a given time increment $\Delta t_{\text{sampling}}$ (or space increment $\Delta x_{\text{sampling}}$), the probability of acceptance P_a of an eddy according to the rate distribution is [17],

$$P_a = \frac{\lambda(r_0, l, t) \Delta t_{\text{sampling}}}{\hat{P}(r_0, l)} \quad \text{or} \quad P_a = \frac{\lambda(r_0, l, x) \Delta x_{\text{sampling}}}{\hat{P}(r_0, l)}. \quad (27)$$

In Eq. (27), specializing for the T-ODT formulation, the acceptance probability is calculated as the ratio of the eddy rate $\lambda(r_0, l, t)$ (in a given sampling time $\Delta t_{\text{sampling}}$) and a presumed eddy size and eddy distribution PDF $\hat{P}(r_0, l)$. This is done following a Poisson process with a mean rate proportional to $\Delta t_{\text{sampling}}$. The derivation of Eq. (27) follows from efficiency considerations regarding the direct sampling from the actual eddy occurrence PDF $P(r_0, l, t)$, defined by the ratio between the local eddy rate $\lambda(r_0, l, t)$ and all of the possible potential eddies with size l and position r_0 at time t , denoted by the global rate $\Lambda = \int \int \lambda(r_0, l, t) dr_0 dl$,

$$P(r_0, l, t) = \frac{\lambda}{\Lambda}. \quad (28)$$

A complete discussion regarding the eddy sampling is given in [17, 18], here we just summarize the most relevant aspects. Indeed, direct sampling from P implies a prohibitively expensive computational cost due to the need to calculate Λ at every given time t . To avoid this, an approximation of the acceptance probability, P_a , is estimated on the basis of a combination of the thinning and rejection methods [16, 24]. Formally, P_a is the product of an acceptance probability based on the thinning method $P_{a,t}$, and an acceptance probability based on the rejection method $P_{a,r}$,

$$P_a = (P_{a,t})(P_{a,r}) = \left(\frac{\Lambda}{n\Lambda} \right) \left(\frac{P}{m\hat{P}(r_0, l)} \right). \quad (29)$$

In the thinning method, eddies are sampled in time as a Poisson process with mean rate $n\Lambda$ ($n > 1$) and then accepted as $\Lambda/n\Lambda$. In the rejection method, eddies are accepted based on the ratio between the unknown P and a presumed PDF $\hat{P}(r_0, l)$ as $P/m\hat{P}$ ($m > 1$, given that $P_{a,r} < 1$). The sampling time interval appearing in Eq. (27) is then taken as $\Delta t_{\text{sampling}} = 1/nm\Lambda$, given the arbitrary nature of the majorizing constants m and n . As commented in [17], $\Delta t_{\text{sampling}}$ is adjusted dynamically during the ODT simulations to achieve an average acceptance probability \bar{P}_a . Also in Eq. (27), $\hat{P}(r_0, l) = f(l)g(r_0)$ is the presumed PDF taken as the product of a uniform distribution for eddy positions $g(r_0)$ and a presumed eddy size PDF $f(l)$, which comprises sizes ranging from the Kolmogorov length-scale to the full domain length, or up to a given threshold L_{max} . Details of the functions $g(r_0)$ and $f(l)$ can be found in [17].

The modeled eddy rate $\lambda(r_0, l, t)$ is based on dimensional analysis considerations and is therefore approximated as $\lambda \sim 1/\tau l^2$. This is a way to relate it to the eddy turnover time τ (characteristic eddy time scale), thus allowing modeling of the energy interactions in the flow. A description of the calculation of λ (or τ) can be found in [14, 18].

We sample eddies with incremental steps $\Delta t_{\text{sampling}}$. Once we find a candidate eddy that is deemed to be implemented according to Eq. (27), we perform a catch-up diffusion process, advancing the diffusion equations detailed in Section 2.1.

We stress that due to the modeling considerations, two model parameters are usually defined, C and Z . In the ODT literature, α is sometimes considered as a model parameter as well. However, due to the theoretical considerations done in Sections 2.2.2 and 3.2, this is not the case for this work. The parameter C is associated to the intensity of the turbulence, while Z is a scaling factor for the magnitude of an energetic viscous penalty that forbids implementation of small eddies, which would otherwise be instantly dissipated [1].

We finalize this section with one last comment regarding an additional step that is commonly done in ODT simulations: the suppression of unphysically large eddies that may occur due to the statistical sampling from the assumed eddy-size PDF. As in [26], we address this topic from the physical point of view of restricting the places where eddies can occur by their maximum length-scale L_{max} . This is based on the assumption of the limitation of the turbulent stirring due to the walls. For multiscale models, as in the case of LES/ODT [26], there is an implicit limitation on L_{max} due to the coupling of the subgrid ODT model in the LES field. For stand-alone ODT calculations in channels or pipes, L_{max} is a parameter that needs to be calibrated. However, we do not consider L_{max} as a model parameter, given that it is not subject to detailed sensitivity studies, i.e. L_{max} values are effectively bounded between 0 and the ODT domain length. By restricting the eddy event size by construction, the Large-Eddy-Suppression mechanism typically done in ODT formulations [1] can be avoided for wall-bounded flows such as channel or pipe flows.

3 Statistical quantities in ODT realizations

As shown in [11], equivalences between statistical DNS and ODT quantities can be made based on the comparison of the mean ODT and Reynolds-Averaged Navier-Stokes (RANS) momentum equations. In this section we review these equivalences from the point of view of Reynolds stresses and Turbulent Kinetic Energy (TKE) budgets for the planar case, summarizing the findings in [11]. Afterwards, we introduce the equivalences for the cylindrical case. For convenience, index notation is used for velocity components in this section.

3.1 Planar Reynolds Stresses and TKE budgets

3.1.1 Planar T-ODT formulation

A mathematical representation of the generalized T-ODT momentum evolution equation in the planar case is given by the differential expression of Eq. (7), with constant density ρ and assumed kinematic viscosity ν ,

$$\frac{\partial u_1}{\partial t} = -\frac{1}{\rho} \frac{\partial \bar{p}}{\partial x} + \nu \frac{\partial^2 u_1}{\partial y^2} + M_1 + K_1. \quad (30)$$

We use $u_1 = u$ in the index notation. $M_1 + K_1$ stands for the combined effect of the triplet-map (M_1), pressure scrambling (S_1) and turbulent transport contribution (T_1) in the ODT velocity component u_1 [11]. According to the definition of the model, K_1 is selected in such a way that $K_1 = T_1 + S_1$, where $S_1 = 0$ is defined for convenience due to the absence of pressure scrambling contributions in the mean Navier-Stokes momentum equation [11]. It is possible to compare Eq. (30) with the steady state channel flow RANS momentum equation,

$$0 = -\frac{1}{\rho} \frac{\partial \bar{p}}{\partial x} + \nu \frac{\partial^2 \bar{u}_1}{\partial y^2} - \frac{\partial \overline{u_1' u_1'}}{\partial y}. \quad (31)$$

Similarly, the mean T-ODT momentum evolution is,

$$\frac{\partial \bar{u}_1}{\partial t} = -\frac{1}{\rho} \frac{\partial \bar{p}}{\partial x} + \nu \frac{\partial^2 \bar{u}_1}{\partial y^2} + \bar{M}_1 + \bar{T}_1. \quad (32)$$

It is then straightforward to verify that the equivalence of the Reynolds stress component $\overline{u_1' u_2'}$ in the T-ODT planar case is given by,

$$-\overline{u_1' u_2'} = \int_{\infty}^y (\bar{M}_1 + \bar{T}_1) dy. \quad (33)$$

Here, the ∞ integration boundary refers to the position of the wall. Operationally, $\bar{M}_1 + \bar{T}_1$ is defined by changes in the velocity profiles due to eddies. Considering the stochastic interaction in Eq. (30) only, within a given interval of time Δt in which an eddy is deemed to occur,

$$\frac{\Delta u_1}{\Delta t} = M_1 + T_1. \quad (34)$$

Averages $\bar{M}_1 + \bar{T}_1$ can then be constructed based on the cumulative sum of changes in the u_1 velocity profiles due to eddies.

For the evaluation of the TKE Budgets, the starting point is the momentum evolution equation, Eq. (30), multiplied by the u_1 velocity component (kinetic energy of the u_1 velocity component),

$$\frac{1}{2} \frac{\partial u_1^2}{\partial t} = -\frac{u_1}{\rho} \frac{\partial \bar{p}}{\partial x} + \nu u_1 \frac{\partial^2 u_1}{\partial y^2} + M_{11} + K_{11} \rightarrow \frac{\partial u_1^2}{\partial t} = -\frac{2u_1}{\rho} \frac{\partial \bar{p}}{\partial x} + \nu \frac{\partial^2 u_1^2}{\partial y^2} - 2\nu \left(\frac{\partial u_1}{\partial y} \right)^2 + M_{11} + K_{11}. \quad (35)$$

Here, $M_{11} + K_{11}$ is the sum of the mapping M_{11} , transport T_{11} and pressure scrambling S_{11} contributions to the kinetic energy of the u_1 velocity component.

Averaging Eq. (35) and using the identities $\overline{u_1^2} - \bar{u}_1^2 = \overline{u_1'^2}$, $I_1 = \int (\bar{M}_1 + \bar{T}_1) dy$, and $I_{11} = \int (\bar{M}_{11} + \bar{T}_{11}) dy$, along with Eq. (32) multiplied by $2\bar{u}_1$, an equation for the average of the square of the fluctuation velocity u_1' can be obtained (see [11] for details),

$$\frac{\partial \overline{u_1'^2}}{\partial t} = \nu \frac{\partial^2 \overline{u_1'^2}}{\partial y^2} - 2\nu \overline{\left(\frac{\partial u_1'}{\partial y} \right)^2} + \left[\frac{\partial}{\partial y} (I_{11} - 2\bar{u}_1 I_1) + \bar{S}_{11} \right] + 2I_1 \frac{\partial \bar{u}_1}{\partial y}. \quad (36)$$

Comparing Eq. (36) to the generalized TKE equation in a Cartesian coordinate system (see, e.g., Eq. (5.164) in [25]), it is possible to deduce that an accurate representation of the flow can be obtained by summing up the contributions by $\overline{u_1'^2}$, $\overline{u_2'^2}$, $\overline{u_3'^2}$, such that $\text{TKE} = (1/2)(\overline{u_1'^2} + \overline{u_2'^2} + \overline{u_3'^2})$. That is, $\alpha \neq 0$ in the ODT model. The most reasonable choice is to consider $\alpha = 2/3$, which implies equal available energy redistribution after an eddy event. The equations for $\overline{u_2'^2}$, $\overline{u_3'^2}$ are similar to Eq. (36), with $\overline{u_2'^2}$, $\overline{u_3'^2}$ substituting $\overline{u_1'^2}$. As in [11], the resulting TKE budgets for production P and dissipation D are,

$$P = \sum_k I_k \frac{\partial \bar{u}_k}{\partial y}, \quad D = \sum_k \nu \overline{\left(\frac{\partial u_k'}{\partial y} \right)^2}. \quad (37)$$

3.1.2 Planar S-ODT formulation

The instantaneous momentum evolution in the spatial formulation is, following from Eq. (12),

$$\frac{\partial u_1^2}{\partial x} = -\frac{1}{\rho} \frac{\partial \bar{p}}{\partial x} + \nu \frac{\partial^2 u_1}{\partial y^2} + M_1 + T_1. \quad (38)$$

Averaging Eq. (38) results in

$$\frac{\partial \overline{u_1^2}}{\partial x} = -\frac{1}{\rho} \frac{\partial \bar{p}}{\partial x} + \nu \frac{\partial^2 \overline{u_1}}{\partial y^2} + \overline{M_1} + \overline{T_1}. \quad (39)$$

Note that in Eq. (38) the averaging procedure neglected the $\partial \overline{u_1' u_1'} / \partial x$ fluctuation term due to the FPG forcing causing a steady flow. In this case, the Reynolds stress component $\overline{u_1' u_2'}$ is also given by Eq. (33). However, in this case, $\overline{M_1} + \overline{T_1}$ is calculated accounting for the changes in the u_1' velocity profiles

$$\frac{\Delta u_1^2}{\Delta x} = M_1 + T_1. \quad (40)$$

The TKE flux equation based on the u_1 velocity component is in this case very similar to the T-ODT formulation. For the spatial formulation, we focus here only on the production and dissipation budgets. Following a similar derivation procedure and accounting for $\alpha = 0$ in the spatial formulation, it is then possible to obtain the corresponding expressions for the production P and dissipation D ,

$$P = I_1 \frac{\partial \overline{u_1}}{\partial y}, \quad D = \nu \overline{\left(\frac{\partial u_1'}{\partial y} \right)^2}. \quad (41)$$

3.2 Cylindrical Reynolds Stresses and TKE budgets

3.2.1 Cylindrical T-ODT formulation

We now introduce for the first time the derivation of the ODT TKE equation for the cylindrical formulation. This derivation allows a very important insight regarding assumptions done in the cylindrical ODT formulation. In order to derive the cylindrical TKE budgets, we follow the same methodology as in the planar case.

The generalized T-ODT cylindrical momentum equation is given in this case by the differential version of Eq. (4),

$$\frac{\partial u_1}{\partial t} = -\frac{1}{\rho} \frac{\partial \bar{p}}{\partial x} + \frac{\nu}{r} \frac{\partial}{\partial r} \left(r \frac{\partial u_1}{\partial r} \right) + M_1 + T_1. \quad (42)$$

Eq. (42) is compared with the steady pipe flow RANS momentum evolution,

$$0 = -\frac{1}{\rho} \frac{\partial \bar{p}}{\partial x} + \frac{\nu}{r} \frac{\partial}{\partial r} \left(r \frac{\partial \overline{u_1}}{\partial r} \right) - \frac{\partial \overline{u_1' u_2'}}{\partial r} - \frac{\overline{u_1' u_2'}}{r}. \quad (43)$$

Here $\overline{u_1' u_2'} = \overline{u' v'}$. Therefore, the mean T-ODT momentum evolution is in this case,

$$\frac{\partial \overline{u_1}}{\partial t} = -\frac{1}{\rho} \frac{\partial \bar{p}}{\partial x} + \frac{\nu}{r} \frac{\partial}{\partial r} \left(r \frac{\partial \overline{u_1}}{\partial r} \right) + \overline{M_1} + \overline{T_1}. \quad (44)$$

Comparing Eqs. (43) and (44), the Reynolds stress component $\overline{u_1' u_2'}$ in the T-ODT cylindrical case is then formally defined by

$$-\overline{u_1' u_2'} = \frac{1}{r} \int_{\infty}^r (\overline{M_1} + \overline{T_1}) r dr = I_1. \quad (45)$$

$\overline{M_1} + \overline{T_1}$ can be calculated just like in the planar case by means of Eq. (34).

The kinetic energy evolution equation for the u_1 axial velocity component is, in this case,

$$\begin{aligned} \frac{1}{2} \frac{\partial u_1^2}{\partial t} &= -\frac{u_1}{\rho} \frac{\partial \bar{p}}{\partial x} + \nu \frac{u_1}{r} \frac{\partial}{\partial r} \left(r \frac{\partial u_1}{\partial r} \right) + M_{11} + K_{11}, \\ \frac{\partial u_1^2}{\partial t} &= -\frac{2u_1}{\rho} \frac{\partial \bar{p}}{\partial x} + \frac{\nu}{r} \frac{\partial u_1^2}{\partial r} + \nu \frac{\partial^2 u_1^2}{\partial r^2} - 2\nu \left(\frac{\partial u_1}{\partial r} \right)^2 + M_{11} + K_{11}. \end{aligned} \quad (46)$$

Analogous to the planar case, the TKE equation based on the u_1 axial velocity component can be obtained as

$$\frac{\partial \overline{u_1^2}}{\partial t} = \frac{\nu}{r} \frac{\partial}{\partial r} \left(r \frac{\partial \overline{u_1^2}}{\partial r} \right) - 2\nu \overline{\left(\frac{\partial u_1'}{\partial r} \right)^2} + \frac{1}{r} \frac{\partial}{\partial r} [r(I_{11} - 2\overline{u_1}I_1)] + 2I_1 \frac{\partial \overline{u_1}}{\partial r} + \overline{S_{11}}. \quad (47)$$

Here, we have used the identity $I_{11} = 1/r \int (\overline{M_{11}} + \overline{T_{11}}) r dr$. A subtraction and addition of $2I_1 \partial \overline{u_1} / \partial r$ is required, just as in the planar case, in order to obtain the final expression.

It is interesting to note that in comparing this expression to the generalized TKE equation in cylindrical coordinates (see, e.g. Eq. (B.31-B.33) in [27]), a series of terms are missing in the model. Unlike in the planar formulation, summing up similar equations for u_2^2 and u_3^2 (radial and tangential velocity fluctuation components) does not result in a more accurate representation of the TKE equation. In a cylindrical coordinate system, the diffusion evolution equations for u_2 and u_3 do not have in general the same terms as u_1 (in contrast to the planar case). In this sense, the budget terms obtained by analyzing Eq. (47) represent only radial fluxes, a radial TKE production term, and interestingly enough, a planar dissipation component. In order to be able to obtain a more accurate representation of the TKE budget terms, different equations for the radial and tangential velocity components would be required, not only in the diffusion evolution PDEs, but possibly in the same eddy implementation procedure. These considerations are valid if the velocity field is interpreted as a vector field, instead of a set of scalars, and if the vector formulation of ODT is used [11]. The scope of this study does not allow further analysis regarding this hypothesis. However, this is an aspect that could be studied in future work.

Due to the before mentioned shortcomings, and in order to guarantee consistency, we conclude in this section that for the case of the cylindrical model formulation, at least in this study, the ODT model parameter α should be set to 0. With this consideration, the radial and tangential velocity components remain 0 and the TKE budgets are consistently represented by Eq. (47) only.

The production and dissipation terms are consequently defined based on Eq. (47),

$$P = I_1 \frac{\partial \overline{u_1}}{\partial r}, \quad D = \nu \overline{\left(\frac{\partial u_1'}{\partial r} \right)^2}. \quad (48)$$

3.2.2 Cylindrical S-ODT formulation

Similar to the temporal formulation, the generalized spatial ODT cylindrical momentum evolution for u_1 is given by

$$\frac{\partial u_1^2}{\partial x} = -\frac{1}{\rho} \frac{\partial \overline{p}}{\partial x} + \frac{\nu}{r} \frac{\partial}{\partial r} \left(r \frac{\partial u_1}{\partial r} \right) + M_1 + T_1. \quad (49)$$

Averaging Eq. (49), results in

$$\frac{\partial \overline{u_1^2}}{\partial x} = -\frac{1}{\rho} \frac{\partial \overline{p}}{\partial x} + \frac{\nu}{r} \frac{\partial}{\partial r} \left(r \frac{\partial \overline{u_1}}{\partial r} \right) + \overline{M_1} + \overline{T_1}. \quad (50)$$

As in the planar case, $\partial \overline{u_1' u_1'} / \partial x = 0$ due to the FPG forcing. Consequently, the Reynolds stress component $\overline{u_1' u_2'}$ is calculated as in the temporal formulation by Eq. (45). The calculation of $\overline{M_1} + \overline{T_1}$ is done exactly as in the planar spatial case via Eq. (40). The production P and dissipation D budgets for $\alpha = 0$ (one velocity component) are given by Eq. (48).

4 Results

4.1 Flow configuration

The details of the simulations performed are given in Tables 1 and 2. All simulations are initialized with constant velocity profiles. Simulations are run without statistical data gathering until the transient effects disappear. Afterwards, online averages and cumulative sums are gathered and updated after eddy events and after diffusion catch-up events, as discussed in Section 3. The data is gathered until the statistical convergence of the desired quantities is achieved.

The ODT code used in this work is the C++ adaptive code developed by D. Lignell [18]. The most important parameters controlling the mesh adaption process are the minimum and maximum cell size allowed during the adaption dx_{min} and dx_{max} , as well as the grid density factor controlling the approximate number of cells generated after the adaption process $gDens$. The factor $gDens$ determines the number of cells to be generated

based on the redistribution calculated by the equipartition of arc lengths in a given adaption interval [17]. These parameters are also given in Tables 1 and 2. Another parameter related to the effects of mesh adaption in the cylindrical formulation, DATimeFac, is explained and evaluated in Section 4.2.

Optimal ODT C and Z parameters are shown in Tables 1 and 2, along with the suggested value of L_{max} for the assumed eddy size PDF used by ODT, as explained in Section 2.2.3. The C and Z parameters were obtained after a model calibration study detailed in Appendix B. Influence due to the assumed value of L_{max} is investigated in Section 4.2, along with the Reynolds number dependence of a numerical parameter associated to mesh adaption, which has so far not been discussed in planar ODT investigations, DATimeFac.

Table 1: Parameters used for channel flow simulations (Temporal and Spatial formulation). η refers to the Kolmogorov length scale.

Parameter (Case)	$Re_\tau = 590$ (A)	$Re_\tau = 934$ (B)	$Re_\tau = 2003$ (C)
Domain Length L (m)	2.0	2.0	2.0
Density ρ (kg/m ³)	1.0	1.0	1.0
Kinematic viscosity ν (m ² /s $\times 10^{-3}$)	1.6949	1.0707	0.9985
FPG Forcing $\partial\bar{p}/\partial x$ (Pa/m)	-1.0	-1.0	-4.0
Mesh adaption parameter $dx_{min} = \eta/3$ (m)	5.6496×10^{-4}	3.5688×10^{-4}	1.6642×10^{-4}
Mesh adaption parameter dx_{max} (m)	0.04	0.04	0.04
Mesh adaption parameter $gDens$	80.0	80.0	80.0
Mesh adaption parameter DATimeFac	4.0	4.0	4.0
ODT parameter C	6.5 (T-ODT) / 3.0 (S-ODT)		
ODT parameter Z	300.0 (T-ODT) / 100.0 (S-ODT)		
ODT parameter α	$2/3 \approx 0.6667$ (T-ODT) / 0.0 (S-ODT)		
Eddy-size PDF L_{max} (normalized by L)	$1/3 \approx 0.3333$		

Table 2: Parameters used for pipe flow simulations (Temporal and Spatial formulation). η refers to the Kolmogorov length scale and Δr_C to the assumed symmetric center cell size.

Parameter (Case)	$Re_\tau = 550$ (A)	$Re_\tau = 1000$ (B)	$Re_\tau = 2003$ (C)
Domain Length $2R$ (m)	2.0	2.0	2.0
Density ρ (kg/m ³)	1.0	1.0	1.0
Kinematic viscosity ν (m ² /s $\times 10^{-3}$)	1.8182	1.0	0.9985
FPG Forcing $\partial\bar{p}/\partial x$ (Pa/m)	-2.0	-2.0	-8.0
Mesh parameter Δr_C (m)	0.04	0.0222	0.0111
Mesh adaption parameter $dx_{min} = \eta/3$ (m)	6.0606×10^{-4}	3.3333×10^{-4}	1.6642×10^{-4}
Mesh adaption parameter dx_{max} (m)	0.04	0.04	0.04
Mesh adaption parameter $gDens$	80.0	80.0	80.0
Mesh adaption parameter DATimeFac	4.0	7.3	14.5
ODT parameter C	5.0 (T-ODT) / 3.0 (S-ODT)		
ODT parameter Z	350.0 (T-ODT) / 100.0 (S-ODT)		
ODT parameter α	0.0		
Eddy-size PDF L_{max} (normalized by $2R$)	$1/3 \approx 0.3333$		

4.2 Sensitivity to L_{max} and DATimeFac parameters

4.2.1 Influence of the parameter L_{max}

As we will show, the qualitative influence of L_{max} on the mean velocity profiles is generally the same in all of the different evaluated friction Reynolds numbers. As shown in [26], L_{max} affects the mean velocity profiles for the channel flow case in the outermost region from the wall. This parameter was estimated to have an optimal normalized value of 0.5 in [26]. [14] also verified the influence of L_{max} on the pipe flow configuration, estimating an optimal normalized value of 0.3333.

Figure 3 shows the influence of L_{max} on the T-ODT formulation for channel and pipe flow. In this study we chose the same value of L_{max} for both the pipe and channel flow configurations, motivated exclusively by consistency between both formulations. We note that it is possible to obtain calibrated parameters that match DNS data with the normalized value of $L_{max} = 0.5$ as in [21, 26], however, we did not do this due to consistency with the cylindrical formulation. It is possible to obtain calibrated parameters that reasonably match DNS data with a normalized value of L_{max} equal to 0.3333 for both the planar and cylindrical configurations. Qualitatively, L_{max} has the same impact in both the channel and pipe flow configurations. Generally speaking, larger values

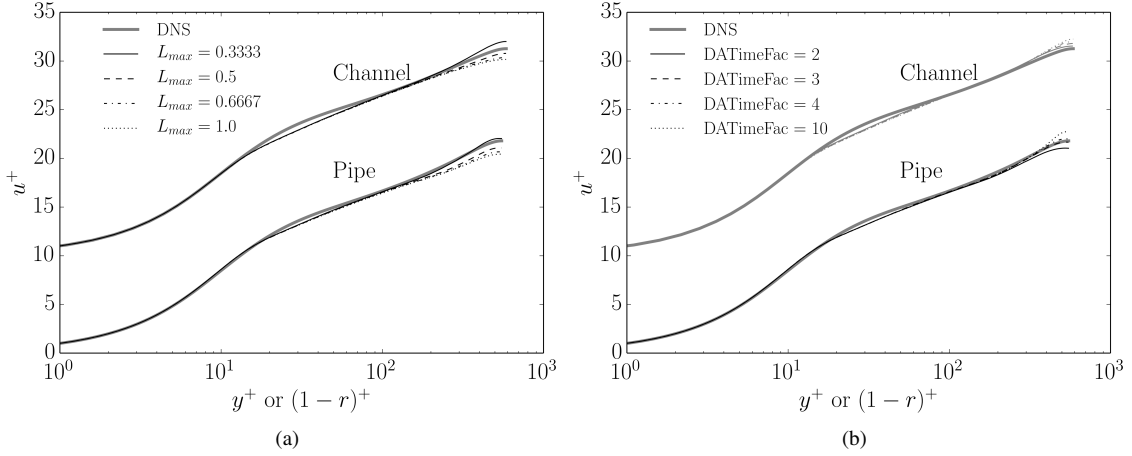


Fig. 3: Influence of the ODT parameters L_{max} and $DATimeFac$ on the normalized wall-normal pipe and channel flow mean velocity profiles. Pipe flow results are shown for $Re_\tau = 550$ and compared to DNS results from [12]. Channel flow results are shown for $Re_\tau = 590$ and compared to DNS results from [23]. Channel flow results have been shifted upwards for better visualization: a) shows the influence of L_{max} and b) the influence of $DATimeFac$.

of L_{max} seem to provoke more mixing close to the centerline, thus resulting in a flatter velocity profile in the centerline surroundings.

4.2.2 Influence of the parameter $DATimeFac$

Despite being seldomly discussed in ODT simulations, one last parameter of interest has been calibrated in this work. This parameter is linked to the performance of the mesh adaption process. Although it was not mentioned in Section 2.2.3, we remark that the diffusion catch-up step characteristic of ODT occurs every time an eddy is implemented, but also anytime that the diffusion CFL time-step Δt_{CFL} is exceeded without any eddy being selected. The diffusion CFL time-step is given by,

$$\Delta t_{CFL} = \frac{dx_{min}^2}{\nu} = \frac{\eta^2}{9\nu}, \quad (51)$$

where dx_{min} is the minimum cell size allowed by the mesh adaption process and η is the Kolmogorov length scale (we assume a resolution $dx_{min} = \eta/3$).

The $DATimeFac$ parameter works as a switch to allow mesh adaption after sufficient time has elapsed without any single eddy being implemented, i.e. time elapsed just performing diffusion steps. For low Reynolds numbers, such as the $Re_\tau = 550$ case evaluated in this work, successive diffusion steps are prone to occur. Also, due to the flow configuration, the probability of eddies being selected in the region close to the centerline is lower. Both of these factors contribute to a larger impact of the mesh adaption process in the region close to the centerline.

Figure 3 shows the influence of $DATimeFac$ in the channel and pipe flow simulations. As in the case of the parameter L_{max} , the influence of $DATimeFac$ is approximately the same for both the channel and pipe-flow configurations. Based on this analysis, we select the value of $DATimeFac = 4$ as the optimal one for all simulations. We note that the influence of $DATimeFac$ is almost negligible in the planar formulation.

Operationally, we can define the $DATimeFac$ as a ratio between a characteristic eddy implementation time-scale and the diffusion CFL time-step. The mesh adaption procedure should be called if we exceed a threshold $\Delta t_d > (DATimeFac) (\Delta t_{CFL})$, where Δt_d is a time interval proportional to some characteristic eddy implementation time-scale. For wall-bounded flows, this characteristic eddy implementation time-scale is proportional to δ/u_τ , the ratio between the half-height of the channel or pipe Radius and the friction velocity.

$$DATimeFac \sim \frac{\Delta t_d}{\Delta t_{CFL}} \rightarrow DATimeFac = \frac{\beta \delta}{u_\tau} \frac{9\nu}{\eta^2}. \quad (52)$$

In Eq. (52) we have substituted Eq. (51) and inserted a proportionality constant β for Δt_d . Eq. (52) allows us to find a scaling law for $DATimeFac$ as a function of the friction Reynolds number, given that $u_\tau = Re_\tau \nu / \delta$. In

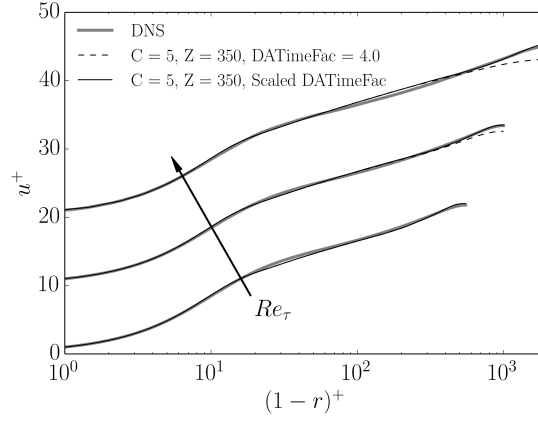


Fig. 4: Influence of DATimeFac scaling on the normalized wall-normal pipe flow mean velocity profile for $Re_\tau = 550, 1000, 2003$. DNS results from [12] ($Re_\tau = 550, 1000$) and [2] ($Re_\tau = 2003$) are shown for reference. The results for increasing Reynolds numbers have been shifted upwards in the plot for better visualization.

fact, it is possible to prove that for a scaling flow regime, such as the one intended with ODT at different Re_τ , the relation between two different DATimeFac factors is,

$$\text{DATimeFac}_2 = \text{DATimeFac}_1 \frac{Re_{\tau,2}}{Re_{\tau,1}}. \quad (53)$$

Therefore we can calibrate the factor DATimeFac for a given $Re_{\tau,1}$ and then find the equivalent DATimeFac₂ corresponding to another $Re_{\tau,2}$. This is the approach followed in this work, where the DATimeFac calibration was performed for Case A in the channel and pipe flow, obtaining the appropriate value of DATimeFac = 4. Evaluating the pipe flow and channel flow configurations, it was found, however, that the planar (channel) configuration was completely insensitive to the DATimeFac scaling with the friction Reynolds number scaling. This is not a surprise, since no planar ODT investigation so far has discussed this parameter. Influence of the scaling was found to be significant in the cylindrical configuration. This can be seen in Figure 4.

We attribute the DATimeFac scaling sensitivity in ODT pipe flow to the center cell treatment, as described in Appendix A and C. The forcing of the fixed center cell size provokes an anomaly caused by the mesh adaption after eddy implementation. This does not occur in the planar formulation. Due to this reason, a delicate balance between the center cell size and the adaption frequency must be considered in order to achieve a consistent scaling, as in the planar formulation.

4.3 Comparison between channel and pipe flow statistics

Statistics gathered from the T-ODT temporal and S-ODT spatial formulation comparing pipe and channel flow simulations are shown in this section. All of the results shown here were obtained with the optimal calibrated parameters presented in Tables 1 and 2.

The ODT spatial formulation developed in this work is thought to be considered as an academic exercise, only for pipe and channel flow, and in principle only to show that both T-ODT and S-ODT formulations are consistent and capable of delivering approximately the same results, something that has never been investigated before. This is a direct analogy of evaluating snapshots in time (for spatially invariant flows) or in space (for temporal invariant flows) with the purpose of constructing average behaviors. For a fully developed flow, such as the pipe and channel flows evaluated in this work, both methods should yield approximately the same statistical results.

The reader should note, however, that simulation times and ODT parameters such as C or Z might vary slightly between the spatial and temporal formulation. This is based on the subtle differences regarding the eddy implementation procedure and the different PDEs that are being solved during the deterministic momentum diffusion evolution. It is also important to stress the fundamental restriction for spatial formulations in ODT, namely, the exclusive treatment of parabolic problems. This leads to simplifications and assumptions made during the derivation of the equations, which are not necessarily the same ones as in the temporal formulation.

Traditional spatial formulations in ODT aim to replicate spatially evolving flows, which would translate, in the context of the pipe and channel flow cases evaluated here, in boundary layer type-flows with a spatially varying friction Reynolds number. This is not the case of the spatial formulation introduced in this work, since we

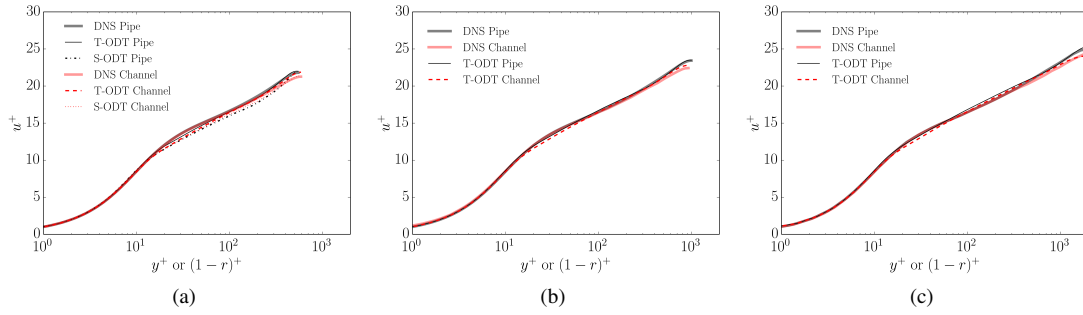


Fig. 5: Normalized wall-normal mean velocity profiles for ODT channel and pipe flow. a) The low friction Reynolds number case (Case A) is shown along with DNS results from [23] (channel) and [12] (pipe). b) Case B results are shown along with DNS results from [6] (channel) and [12] (pipe). c) Case C results are shown along with DNS results from [6] (channel) and [2] (pipe).

are using a FPG forcing. For this reason, our spatial simulations resemble the temporal simulations: an ensemble average over realizations at a same spatial coordinate is exactly equivalent to an ensemble average over accumulated realizations in space. The latter is the averaging philosophy applied in this work for the spatial simulations. In the temporal simulations, an ensemble average over accumulated realizations in time is considered.

4.3.1 Mean velocity profiles and RMS velocity profiles

The results for the normalized wall-normal mean velocity profile are summarized in Figure 5 for the different Reynolds numbers evaluated in this work. Note that, as in the DNS from [2] and due to the available DNS results in the literature, the friction Reynolds numbers from $Re_\tau = 590$ and $Re_\tau = 934$ for the channel flow simulations are compared to the $Re_\tau = 550$ and $Re_\tau = 1000$ pipe flow simulations. Although the Reynolds numbers are not exactly the same ones, the differences in the comparison are expected to be negligible.

As it has been shown previously for channel flow simulations [21, 26], ODT reasonably reproduces the mean velocity profile behavior. The comparison between DNS and ODT data for pipe flow and channel flow shows that ODT simulations are able to match the DNS behavior very well in the viscous layer, the inner buffer layer and the logarithmic layer. Differences can be noted between ODT and DNS in the meso layer and outer buffer layer. These differences are expected, since the buffer layer is mainly influenced by large scale structures not represented in ODT (see [21] for details).

By comparing ODT results between pipe and channel flow simulations, it is immediately noticeable that the similarity of the flows is maintained, just as in the DNS. Considering that the recent cylindrical formulation in ODT has not undergone significant validation studies, this is an aspect worth stressing. Also, the similarity of the channel and pipe flows is somehow reflected on the chosen optimal C and Z values for the planar and cylindrical configurations, given that these values lie very close to each other. As it is seen in the DNS results, the ODT behavior for channel flow shows an earlier departure into the logarithmic layer in comparison to pipe flow.

Based on the results obtained for case A, where no remarkable improvement was achieved in the results by using the spatial formulation, no further calculations for case B or C were done using the S-ODT formulation. This does not mean that the spatial formulation is not worth studying. In principle, the spatial formulation for closed lines is an alternative to the T-ODT formulation and it is able to match its results, even when there could be significant room for improvement, given the limitations which were discussed in previous sections (e.g. $\alpha = 0$). With the optimal parameters selected for the spatial formulation, the obtained mean velocity profile for case A lies below the one of the temporal formulation in the logarithmic and outer buffer layers. Note that these results were obtained just by tuning the C and Z parameters in order to achieve a reasonable match in the case A simulations. The same L_{max} and DATimeFac parameters from the temporal formulation were used for the spatial formulation.

It is also interesting to note that, at least for case A, the optimal values for the parameters C and Z are the same ones for both the pipe and channel flow configurations in the spatial formulation ($C = 3.0$ and $Z = 100.0$).

A comparison of the RMS velocity profiles for ODT and DNS channel and pipe flow simulations is shown next in Figure 6. In contrast to the mean velocity profiles, the ODT behavior is significantly different from the DNS data, however, this is something that has been already verified in previous ODT investigations (see [17, 21]). In the viscous layer, ODT results are slightly shifted in a parallel manner compared to DNS results. Discrepancies between ODT and DNS become more pronounced after the RMS peak close to the wall is achieved. ODT results for channel and pipe flow show similar behavior. The RMS double peak in T-ODT results is an intrinsic feature of

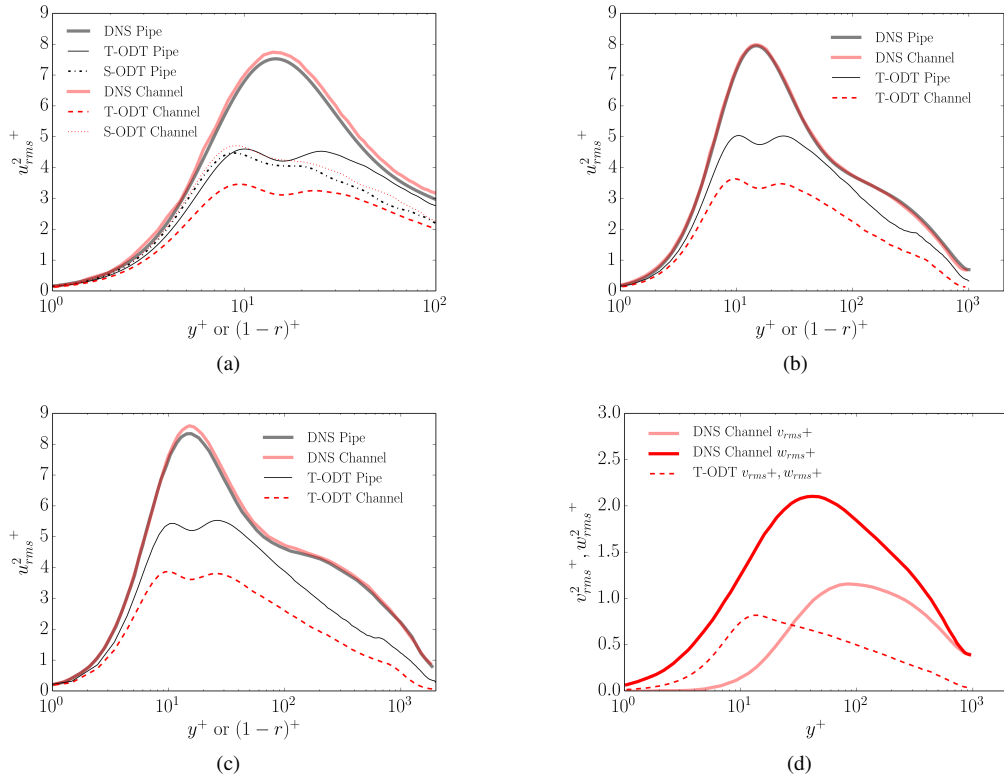


Fig. 6: Normalized wall-normal RMS velocity profiles for ODT channel and pipe flow. (a): the low friction Reynolds number case (Case A) is shown along with DNS results from [23] (channel) and [12] (pipe). (b): Case B results are shown along with DNS results from [6] (channel) and [12] (pipe). (c): Case C results are shown along with DNS results from [6] (channel) and [2] (pipe). (d): Case B results for channel crosswise and spanwise RMS velocity profiles compared to DNS results from [6].

the model [17], and it must not be confused with the common second peak discussion for pipe flow simulations in large Reynolds numbers regimes [2, 19]. We note that the double peak obtained in the S-ODT formulation is significantly reduced and almost disappears from the profile. This could be seen as an advantage against the temporal formulation. However, the position of the peak in the spatial formulation is shifted in comparison to the DNS results.

Since the ODT parameter α was set to 0 in the pipe flow T-ODT simulations (and must be 0 in the S-ODT simulations), the only RMS velocity profiles that can be obtained from the model are those shown in Figure 6 (velocity profiles for the streamwise velocity component). $\alpha = 0$ also implies that the kinetic energy is fully contained in the streamwise velocity component, explaining why the RMS profiles for pipe flow ODT simulations lie above the ones for channel flow simulations. For the channel flow case in the T-ODT formulation, we used $\alpha = 2/3$, thus we show also in Figure 6 the results for the u_2 and u_3 (v, w) velocity components in ODT (these results are shown for $Re_\tau = 934$, case B). Both v and w velocity components have the same magnitude in ODT in this case. This is due to the model formulation with $\alpha = 2/3$ and equal initial conditions for both velocity components.

Figure 7 shows a comparison of the pre-multiplied mean velocity gradient for Case B using the temporal formulation. In this case, channel DNS results from [8] for $Re_\tau = 1000$ and pipe DNS results from [12] for $Re_\tau = 1000$ were available and used for the comparison. Although the plot dispersion is pronounced in regions far away from the wall, some general trends from the DNS data [2] are confirmed with ODT. In both DNS and ODT, there is no constant region of pre-multiplied velocity gradient beyond the point of departure, which indicates that the logarithmic law does not hold for this case. It is known that such constant profile in the pre-multiplied velocity gradient only starts to appear in fairly large Reynolds numbers regimes [12]. The trends from Case B are also reproduced for Case C in the current simulations without any noticeable difference (not shown here). At least for channel flow, as shown in [15], the constant profile region for the pre-multiplied velocity gradient starts appearing around $Re_\tau \approx 4200$, a friction Reynolds number which was out of scope for this work.

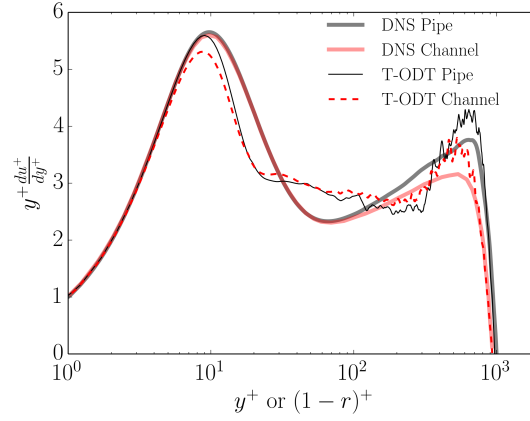


Fig. 7: Comparison of the pre-multiplied mean velocity gradient for the channel and pipe flow case B simulations. DNS results from [8] (channel) and [12] (pipe) are shown for reference.

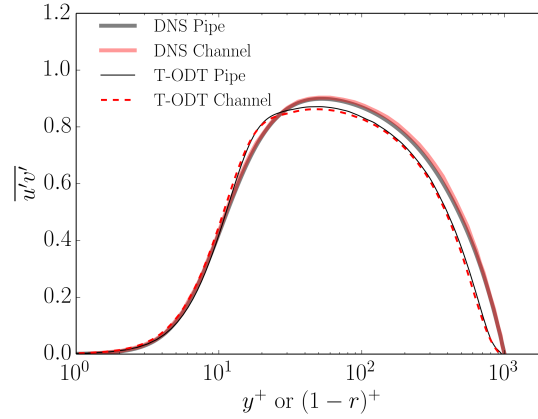


Fig. 8: Cross-wise Reynolds stress component $\overline{u'v'}$ for T-ODT Case B simulations. DNS results from [15] (channel) and [12] (pipe) are shown along for comparison.

4.3.2 TKE Budgets

Following the methodology explained in Section 3, results concerning the calculation of the Reynolds stresses and the TKE budgets are shown next.

Figure 8 shows the Reynolds stress component $\overline{u'v'}$ in the channel and pipe flow T-ODT simulations and its comparison to DNS data. The figure shows that it is possible to achieve a remarkable match between ODT and DNS results. One point worth stressing is that the calculations done according to Section 3, gathered statistical data only from one side of the domain for the pipe flow case. The reason behind this methodology is that, unlike the solution of the momentum PDEs that was carried out by means of an integral formulation in a FVM, the derivation of the TKE budgets equation was done entirely in differential terms. Thus, a Finite Difference Method (FDM) discretization was used and the origin $r = 0$ had to be avoided. The results for the Reynolds stress show that the ODT model is effectively able to reproduce the energetic interactions in both the channel and pipe-flow simulations. The reader should note that the terminology of the Reynolds stresses used here is the one corresponding to the calculation methods in Section 3. These Reynolds stresses should not be confused with the RMS velocity values, e.g. in the case of $\overline{v'v'} \neq v_{rms}^2$. The latter is calculated only as $v_{rms}^2 = \overline{v^2} - \bar{v}^2$ and does not have an inherent meaning in ODT, unlike the Reynolds stress $\overline{v'v'}$ [10].

The comparison of the TKE budgets for production and dissipation between the pipe and channel flow simulations is shown in Fig. 9 for Case B. In this case, as it has been shown with the previous results, there is again reasonable agreement between DNS and ODT results. The TKE production is remarkably well reproduced by ODT for both the pipe and channel flow cases. This is not a surprise given the agreement of the Reynolds stresses and the mean velocity profiles shown before. In the case of the TKE dissipation, both ODT results for channel and pipe agree very well with each other, but show some discrepancies with DNS results. The agreement in both ODT

cases is also non-surprising, given the fact that the TKE dissipation budget solved for the cylindrical formulation is planar, as it was explained in Section 3. The departure between ODT results and DNS for the TKE dissipation budget, at least in the temporal formulation, is not new and has been extensively discussed [21, 26].

We focus our attention now on the results obtained with the spatial formulation for the TKE production and dissipation budgets. Figure 9 also shows a comparison for the results obtained with the spatial and temporal formulations of pipe and channel flow. The production budget from the spatial formulation matches perfectly the results obtained with the temporal formulation. The dissipation budget, however, despite achieving agreement in the values next to the wall and away from it, shows increased values between $y^+ \approx 10$ and $y^+ \approx 40$. This region of increased dissipation is in agreement with the region of dissimilar behavior between the temporal and spatial formulation in the streamwise RMS velocity profile. Thus, the increased dissipation in this area is apparently an artifact in the spatial formulation that erodes the second peak in the ODT streamwise turbulence intensity.

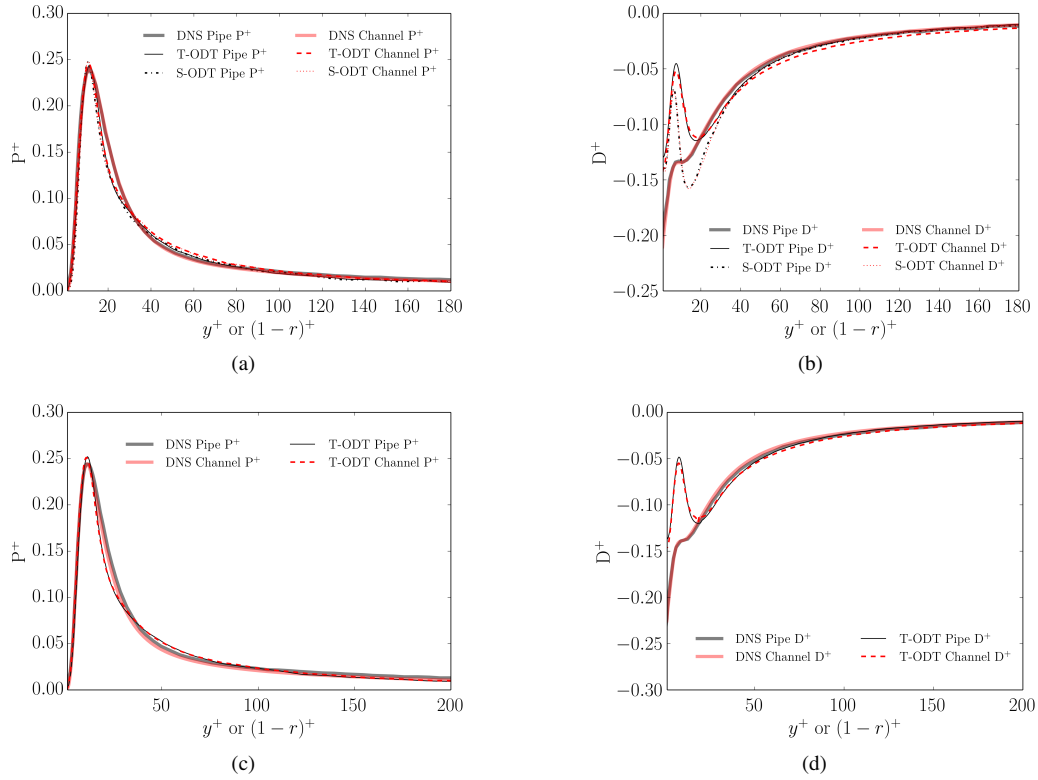


Fig. 9: TKE Production (P^+) and Dissipation (D^+) budgets for T-ODT (cases A and B) and S-ODT (case B) simulations. DNS results from [23] (channel) and [12] (pipe) are shown for reference in case A, while results from [15] (channel) and [12] (pipe) are shown for comparison in case B. (a) Production budget in case A. (b) Dissipation budget in case A. (c) Production budget in case B. (d) Dissipation budget in case B.

5 Conclusions

A detailed study of the cylindrical ODT formulation was carried out in this work. In contrast to the general framework for the cylindrical formulation presented in [18], an exhaustive analysis of the ODT dynamics for cylindrical pipe flow has been done, considering the traditional T-ODT formulation. Additionally, a novel spatial formulation for the channel and pipe flow configurations was introduced, as a demonstrative way to prove the consistency of the temporal and spatial formulations, at least in channel and pipe flows, therefore illustrating the capabilities of the model, while simultaneously presenting new ways to potentially improve results.

Results for the stand-alone ODT model in both its temporal and newly introduced spatial formulations for pipe and channel flows were shown to be able to achieve satisfactory results whenever compared with DNS data. Replicability of the DNS data for the wall-normal mean velocity profiles was obtained for all of the formulations, and a calibration process to achieve Reynolds number independent parameters was successfully carried out for

the temporal formulation. In general, both the planar and cylindrical ODT formulations are also able to replicate with great accuracy the flow energetics, as shown by the obtained pre-multiplied velocity gradient and cross-wise Reynolds stress behavior. Despite the discrepancies between ODT and DNS results, it was shown that ODT is able to capture most of the dynamics in wall-bounded flows.

Also, despite the solid results shown for the cylindrical formulation in this work, we proved theoretically that the current formulation of the model is only able to reproduce radial fluxes and mimick a planar TKE dissipation term. Although this proved sufficient for this work, it also implies that there is room for improvement in further studies.

Although it was not the main motivation of this work to prove the efficiency of the ODT model against the DNS method, we stress that all of the ODT simulations carried out for this work used, independently, one core of an Intel i7-2600 CPU with 3.4 GHz and 8GByte memory, working in the most severe cases with around 2000 grid points. As a reference, the nek5000 pipe flow code used in [12] required 2.1842×10^9 grid points and employed an available infrastructure of 65,536 cores.

Disclosure of potential conflicts of interest

Conflict of Interest: The authors declare that they have no conflict of interest.

Acknowledgements The authors would like to acknowledge the financial support from the European Funds for Regional Development (EFRE-Brandenburg). This work was carried out within the framework of the project 'Einsatz elektrohydrodynamisch getriebener Strömungen zur erweiterten Nutzung von Elektroabscheidern'. Partial support was also provided by the U.S. National Science Foundation under grant number CBET-1403403. The authors also acknowledge the valuable discussions regarding the vector and scalar approaches in ODT motivated by Alan Kerstein during the realization of this work.

A Appendix: Discretization and numerical method for momentum diffusion evolution

A.1 T-ODT formulation

The discretization and numerical advancement of the diffusion evolution PDEs is discussed in this section. The FVM for the integral momentum pipe flow equation, Eq. (4), is obtained by discretization of the r dimension, considering grid cells i with cell interfaces at $i + 1/2$ and $i - 1/2$ (integrals are evaluated within these limits). Constant properties are assumed within cells and the density is a constant. This leads to the discretized equation,

$$\rho \left(\frac{\partial u}{\partial t} \right)_i (r_i \Delta r_i) = - \frac{\partial \bar{p}}{\partial x} (r_i \Delta r_i) + \left[\left(r_{i+1/2} \mu \frac{u_{i+1} - u_i}{r_{i+1} - r_i} \right) - \left(r_{i-1/2} \mu \frac{u_i - u_{i-1}}{r_i - r_{i-1}} \right) \right]. \quad (54)$$

We note that $r_i \Delta r_i = [(r_{i+1/2} + r_{i-1/2})/2](r_{i+1/2} - r_{i-1/2}) = (r_{i+1/2}^2 - r_{i-1/2}^2)/2$, which is the same as the result of the integral $\int r dr$ in the cell i , i.e. the radial area/volume of the cell i .

For the case $r_i = 0$, Eq. (54) contains an apparent singularity if the factor $r_i \Delta r_i$ is rearranged to divide the RHS. The singularity treatment for pipe flow numerical simulations is an old and known problem. In the DNS field, the singularity treatment reduces commonly to one of two approaches: either the discretization is done by effectively suppressing the singularity through the transformation of the cylindrical equations to a polynom-based Spectral Element Method (SEM) (see, e.g. [12]), or by avoiding the singularity with a special FVM treatment [3]. In this work we have chosen the latter approach. Given that the ODT line mesh is non-uniform, there are three possible choices regarding the cell that contains the position $r = 0$:

- The cell contains the position $r = 0$ at the face (either $r_{i+1/2}$ or $r_{i-1/2}$ are 0).
- The cell is symmetric and contains the position $r_i = 0$ at its center.
- The cell is asymmetric and contains the position $r = 0$.

Examining Eq. (54) discretized with an explicit method, it should be noted that the 1st option of our list of choices must be discarded, since neglecting either $r_{i+1/2}$ or $r_{i-1/2}$ would effectively neglect the influence of one side of the domain on the other side during the time advancement. This choice is somehow damped, but not entirely removed by choosing the 3rd option of the list. Using the 2nd option in the list with an explicit method supposes another problem, given that the time-derivative is zero due to the factor $r_i \Delta r_i$ when $r_i = 0$. The way then to circumvent this issue is to apply an implicit method along with a symmetric center cell.

If Eq. (54) is discretized with a backward Euler method solved by means of a Tridiagonal Matrix Algorithm (TDMA), the communication between cells allows the construction of a matrix in which the disappearance of the time derivative factor on the LHS of the equation results in a shear stress flux equalization condition,

$$\left(r_{i+1/2} \mu \frac{u_{i+1} - u_i}{r_{i+1} - r_i} \right) = \left(r_{i-1/2} \mu \frac{u_i - u_{i-1}}{r_i - r_{i-1}} \right). \quad (55)$$

This expression implies, that within the center cell, there is no net gain or loss of momentum (the incoming fluxes necessarily cancel out the outgoing fluxes). This is similar to the axis averaging methods used by DNS (see [3]). Also, by solving Eq. (54) with an implicit method, any discussion regarding the nature of the diffusion CFL condition in cylindrical coordinates is avoided.

The reader is advised at this point that this implicit solution procedure is not exactly the same one done in [18], where the momentum equation was solved explicitly due to a different treatment of the diffusion in the center cell. In [18], the center cell term

$r_i \Delta r_i = (r_{i+1/2}^2 + r_{i-1/2}^2)/2$, given that $r_{i-1/2}$ and $r_{i+1/2}$ have opposite signs due to the treatment of the coordinate system with $r \in \mathbb{R}$. This is also the result of the integral $\int r dr$ evaluated from 0 to $r_{i+1/2}$ multiplied by 2, which is the factor accounting for an integration over an arc 2π , normalized by π , instead of the standard integration over $\Delta\theta$ for any other disc ring that does not contain the origin. Therefore, in [18], the singularity is also avoided and an explicit method along with a symmetric center cell is used.

Given that the ODT code used is adaptive, the symmetric center cell implementation encounters a problem that is circumvented by forcing the symmetric center cell with fixed size after every mesh adaption call. This causes strong sensitivity with the mesh adaption, an aspect discussed in Section 4.2. The center cell is considered to have a size equal to dx_{\max} (mesh adaption parameter) in the calibration case $Re_\tau = 590$. Assuming that this center cell is also proportional to the Kolmogorov length scale, we scale the size of the center cell with different friction Reynolds numbers as,

$$\frac{\Delta r_{C,1}}{\Delta r_{C,2}} = \frac{\beta \frac{v_1}{u_{\tau,1}}}{\beta \frac{v_2}{u_{\tau,2}}} \rightarrow \Delta r_{C,2} = \Delta r_{C,1} \frac{Re_{\tau,1} \delta_2}{Re_{\tau,2} \delta_1}. \quad (56)$$

In Eq. (56), β is a proportionality constant to relate the center cell size Δr_C with η , where η is the Kolmogorov length scale estimated as v/u_τ . This consideration is done in order to scale the center cell size as the scaling of the Kolmogorov length scale, although they do not have the same magnitude. u_τ is obtained from the friction Reynolds number definition, which involves δ as the pipe radius.

For the case of T-ODT channel flow, the advancement of the momentum diffusion evolution by Eq. (7) does not require any special treatment. This is carried out in this work by means of a forward Euler explicit method, considering the diffusion CFL condition. The spatial discretization is given by,

$$\rho \left[\frac{\partial u}{\partial t} \right]_i = -\frac{\partial \bar{p}}{\partial x} + \frac{1}{\Delta y_i} \left[\left(\mu \frac{\partial u}{\partial y} \right)_{i+1/2} - \left(\mu \frac{\partial u}{\partial y} \right)_{i-1/2} \right], \quad (57)$$

A.2 S-ODT formulation

For the S-ODT pipe flow numerical advancement, some additional considerations in comparison to the temporal formulation must be taken into account. The S-ODT pipe flow case is perhaps the most challenging one in this work, since not only the same considerations of the temporal formulation must be followed (the equation must be solved implicitly), but also due to the presence of the u^2 term that needs to be advanced according to Eq. (10).

In this case, Eq. (10) is discretized implicitly as follows, considering the density as a constant,

$$\rho \frac{u_i^{2,n+1} - u_i^{2,n}}{\Delta x} (r_i \Delta r_i) = -\frac{\partial \bar{p}}{\partial x} (r_i \Delta r_i) + \left[\left(r_{i+1/2} \mu \frac{u_{i+1} - u_i}{r_{i+1} - r_i} \right) - \left(r_{i-1/2} \mu \frac{u_i - u_{i-1}}{r_i - r_{i-1}} \right) \right]^{n+1}. \quad (58)$$

In Eq. (58), the superindexes n and $n+1$ refer to the spatial positions x_n and x_{n+1} . The backward Euler implicit formulation for the LHS spatial derivative was also used. This equation is solved using the Babylonian method [4], which is a simplification of the general Newton's method. In the Babylonian method, if a is an approximation to \sqrt{N} , then the average $1/2(a + N/a)$ is a better approximation to \sqrt{N} . Applying this definition to our discretized Eq. (58), we compute iteratively the velocity u^{n+1} as,

$$u_i^{n+1} = \frac{1}{2} \left\{ u_i^* + \frac{u_i^{2,n} (r_i \Delta r_i) - \frac{\Delta x}{\rho} \frac{\partial \bar{p}}{\partial x} (r_i \Delta r_i) + \frac{\Delta x}{\rho} \left[\left(r_{i+1/2} \mu \frac{u_{i+1} - u_i}{r_{i+1} - r_i} \right) - \left(r_{i-1/2} \mu \frac{u_i - u_{i-1}}{r_i - r_{i-1}} \right) \right]^{n+1}}{u_i^* (r_i \Delta r_i)} \right\}. \quad (59)$$

Here, a value of u_i^* is assumed (first guess is $u_i^* = u_i^n$). A standard implicit TDMA is used to obtain values of u_i^{n+1} with constant value of u_i^* . After this is done, the value of u_i^* is updated to the value just found for u_i^{n+1} . This procedure is repeated until the residual between two consecutive obtained values of u_i^{n+1} satisfies a given tolerance. We find convergence up to a tolerance approximately equal to 1×10^{-10} m/s determined using a maximum norm in about 5 iterations (as a comparison value for the error tolerance, we consider a reference value of u_τ of 1 m/s).

For the S-ODT channel flow, the advancement is done analogous to the cylindrical formulation, by the formula,

$$u_i^{n+1} = \frac{1}{2} \left\{ u_i^* + \frac{u_i^{2,n} (\Delta y_i) - \frac{\Delta x}{\rho} \frac{\partial \bar{p}}{\partial x} (\Delta y_i) + \frac{\Delta x}{\rho} \left[\left(\mu \frac{u_{i+1} - u_i}{y_{i+1} - y_i} \right) - \left(\mu \frac{u_i - u_{i-1}}{y_i - y_{i-1}} \right) \right]^{n+1}}{u_i^* (\Delta y_i)} \right\}. \quad (60)$$

We note that it would also be possible to advance the planar spatial formulation explicitly as in the temporal formulation, accounting for the advanced quantity u^2 instead of u in Eq. (12). Except for the $\partial/\partial x$ derivative term, the discretization formula for the advancement would be the same as in Eq. (57). The application of a square root operator should follow after the time-stepping to find the value of u , whereby the positive root should be considered at all times. This is due to the use of the FPG forcing, which, altogether with the assumption of the preservation of the 1-D kinetic energy spectrum ($\alpha = 0$ during an eddy event) guarantees that the velocity field is positive everywhere and at all times.

None of the procedures described here for solving the spatial formulation are the same ones as that used by Lignell et al in [17] and [18], which is a spatial formulation for open lines. In the before mentioned studies, a non-conservative version of the momentum equation is used, by replacing $\partial u^2/\partial x$ by $u \partial u/\partial x$ due to the substitution of the continuity equation (see [18] for details). We omit this substitution, in an effort to work with a formally conservative formulation. In any case, continuity is a condition that does not need to be solved for closed lines with constant density, as discussed in Section 2.1.2.

B Appendix: Calibration of the model parameters C and Z for the T-ODT simulations

As in any turbulence model, some degree of empiricism is associated with ODT. In our study, this empiricism is related to the determination of the values for the parameters C and Z of the model. On one hand, the C parameter is directly related to the frequency of events being implemented, i.e. the turbulence intensity [1]. On the other hand, the Z parameter is seen as a factor which might effectively deny the implementation of an eddy event. Z is primarily a cutoff mechanism for eddies that, if implemented, might be instantaneously dissipated as heat, thus having essentially no impact in the flow dynamics. Initial values for C and Z for the T-ODT channel and pipe flow simulations were selected based on the evaluations carried out in [17] and [14] respectively. These values were then subject to a sensitivity study in order to determine the optimal values used in this work (values in Tables 1 and 2).

Figure 10 exemplifies the impact of different C and Z values on T-ODT pipe flow simulations, specifically on the normalized wall normal mean velocity profile. In general, reducing the value of C decreases the number of eddies being implemented and causes a profile behavior closer to the laminar one. Reducing the value of C implies a shift in the logarithmic region towards higher velocity values. This is represented by a moderate increase in the slope of the mean velocity profile in the outer layer.

Traditional evaluations of the Z parameter in ODT identify it as an order unity model parameter [1]. For the case of wall-bounded flows [14, 17, 21] and recent boundary layer investigations [5], this has been proven as an inadequate generalization. For two-sided wall bounded flows such as the channel and pipe flow configurations evaluated here, the three-dimensional effects of flow structures living in the buffer layer of the flow might be responsible of a significant departure from the ODT model hypothesis. In these cases, Z is instead used in ODT as a tunable cutoff parameter intended to mimick the true behavior of the flow dynamics. In general, increasing the value of Z shifts the logarithmic region of the mean velocity profile upwards, but preserves the slope of the profile. Reducing the value of Z is seen to cause an earlier departure of the velocity profile towards the logarithmic region [5].

Given the tunable nature of the C and Z coefficients, there are different combinations of these parameters that might reproduce different aspects of the flow dynamics. It is possible that a chosen pair of values for C and Z allows good reproducibility of the mean velocity profiles, but not optimal results for the Reynolds stresses [5]. It is also possible that there is more than one pair of values for C and Z that reproduces with reasonable accuracy the true flow dynamics in the mean velocity profile. In the case of this study, we select the optimal values for C and Z based on their effect over the mean velocity profile for the different friction Reynolds numbers given in Tables 1 and 2. Following the ODT philosophy, the ultimate goal of this calibration process is to achieve a Reynolds number independence of the calibration parameters.

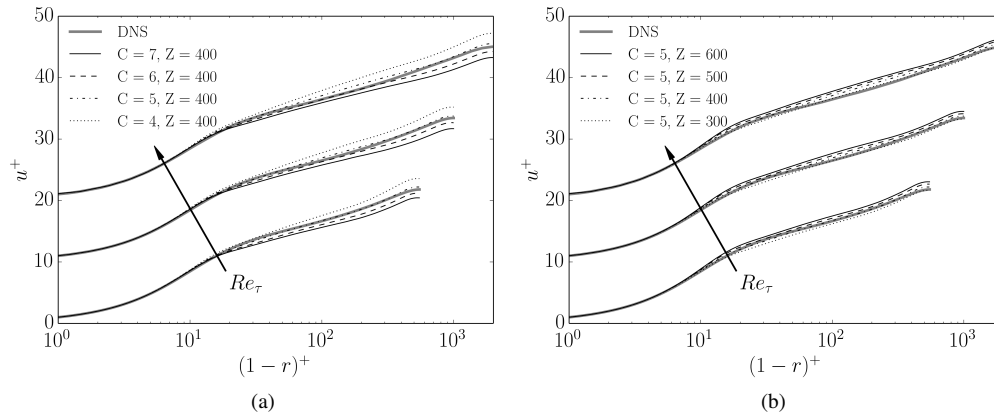


Fig. 10: Influence of the ODT model parameters on the normalized wall-normal pipe flow mean velocity profile for $Re_\tau = 550, 1000, 2003$. DNS results from [12] ($Re_\tau = 550, 1000$) and [2] ($Re_\tau = 2003$) are shown for reference. The results for increasing Reynolds numbers have been shifted upwards in the plot for better visualization. a) Influence of C and b) Influence of Z

C Appendix: Centerline anomaly in pipe flow RMS velocity profiles

During the numerical simulations for pipe flow performed in this work, evidence of anomalous activity around the centerline for the RMS velocity profiles was found for the low Reynolds number case, even when implementing the before discussed center cell treatment. There seems to be a delicate balance of model parameters in pipe flow simulations, which however, can be properly scaled based on all considerations discussed in this paper. We note that this anomaly is also exaggerated due to the use of the Triplet Map A formulation (TMA), in comparison to the TMB formulation used by [18]. As explained in [18], in comparison to the TMB formulation, the TMA has a more pronounced spike of the normalized inverse eddy turnover time τ^{-1} in the proximity of $r = 0$. The fact that τ^{-1} first drops at a normalized distance around $2r/l$ and then surges in the proximity to $r = 0$ in TMA, implies that eddies are favored to occur at $r = 0$, but discouraged in the proximity of $r = 0$ up to $2r/l$ [18].

In the mean velocity profiles, this is seen as the relative jump of the profile towards the centerline, where mixing does not take place due to eddies dominantly centered at $r = 0$. Based on this, the dependence on DATimeFac is also justified, given that in order to match the mean velocity profile, we seek a mechanism to introduce more diffusion around the centerline, where the mixing is disproportionate in comparison to the mixing happening right at the center in $r = 0$. This also justifies a dependence on L_{max} for the cylindrical formulation, given that whenever eddies are approximately of size R , the center parcels can be mixed. Influence to L_{max} and DATimeFac was discussed in Section 4.2 from the point of view of the mean velocity profiles, however, the reader can see in

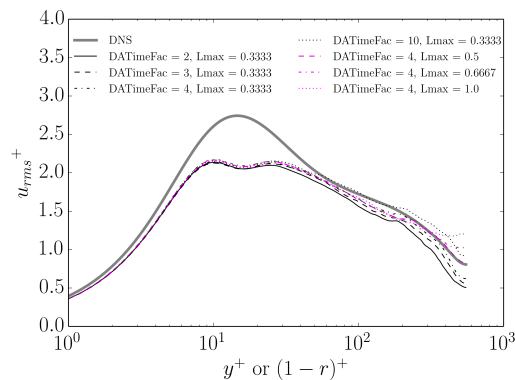


Fig. 11: Centerline anomaly sensitivity to L_{max} and DATimeFac parameters.

Figure 11, the effect that these parameters have on the RMS velocity profiles. A proper combination of L_{max} and DATimeFac is able to alleviate this centerline anomaly in ODT, which arises due to the characteristics of the cylindrical formulation.

References

1. Ashurst, W., Kerstein, A.: One-dimensional turbulence: Variable-density formulation and application to mixing layers. *Phys. Fluids* **17** (2005). DOI 10.1063/1.1847413
2. Chin, C., Monty, J., Ooi, A.: Reynolds number effects in DNS of pipe flow and comparison with channels and boundary layers. *Int. J. Heat Fluid Flow* **45**, 33–40 (2014)
3. Eggels, J.G.M.: Direct and Large Eddy Simulation of Turbulent Flow in a Cylindrical Pipe Geometry. Ph.D. thesis (1994)
4. Fowler, D., Robson, E.: Square Root Approximations in Old Babylonian Mathematics: YBC 7289 in Context. *Historia Mathematica* **25**(HM982209), 366–378 (1998)
5. Fragner, M., Schmidt, H.: Investigating asymptotic suction boundary layers using a one-dimensional stochastic turbulence model. *Journal of Turbulence* **18**(10) (2017). DOI 10.1080/14685248.2017.1335869
6. Hoyas, S., Jimenez, J.: Scaling of the velocity fluctuations in turbulent channels up to $Re_\tau = 2003$. *Phys. Fluids* **18**(011702) (2006)
7. Hultmark, M., Vallikivi, M., Bailey, S.C.C., Smits, A.J.: Turbulent Pipe Flow at Extreme Reynolds Numbers. *Phys. Rev. Lett.* **108**(094501) (2012)
8. Jimenez, J., Hoyas, S., Simens, M., Mizuno, Y.: Turbulent boundary layers and channels at moderate Reynolds numbers. *J. Fluid Mech.* **657**, 335–360 (2010)
9. Jozefik, Z., Kerstein, A., Schmidt, H., Lyra, S., Kolla, H., Chen, J.: One-dimensional turbulence modeling of a turbulent counter-flow flame with comparison to DNS. *Combust. Flame* **162**, 2999–3015 (2015)
10. Kerstein, A.: One-dimensional turbulence: model formulation and application to homogeneous turbulence, shear flows, and buoyant stratified flows. *J. Fluid Mech.* **392**, 277–334 (1999)
11. Kerstein, A., Ashurst, W., Wunsch, S., Nilsen, V.: One-dimensional turbulence: Vector formulation and application to free-shear flows. *J. Fluid Mech.* **447**, 85–109 (2001)
12. Khoury, G., Schlatter, P., Noorani, A., Fischer, P., Brethouwer, G., Johansson, A.: Direct Numerical Simulation of Turbulent Pipe Flow at Moderately High Reynolds Numbers. *Flow, Turbul. Comb.* **91**, 475–495 (2013)
13. Kim, K., Adrian, R.: Very large-scale motion in the outer layer. *Phys. Fluids* **11**(2), 417–422 (1999)
14. Krishnamoorthy, N.: Reaction Models and Reaction State Parametrization for Turbulent Non-Premixed Combustion. Ph.D. thesis, University of Utah (2008)
15. Lee, M., Moser, R.: Direct Numerical Simulation of turbulent channel flow up to $Re_\tau = 5200$. *J. Fluid Mech.* **774**, 395–415 (2015)
16. Lewis, P.A., Shedler, G.S.: Simulation of nonhomogeneous Poisson process by thinning. *Naval Res. Logistics Quart.* **26**, 403–413 (1979)
17. Lignell, D., Kerstein, A., Sun, G., Monson, E.: Mesh adaption for efficient multiscale implementation of One-Dimensional Turbulence. *Theoretical and Computational Fluid Dynamics* **27**(3-4), 273–295 (2013). DOI 10.1007/s00162-012-0267-9
18. Lignell, D., Lansinger, V., Medina M., J.A., Kerstein, A., Schmidt, H., Fistler, M., Oevermann, M.: One-dimensional turbulence modeling for cylindrical and spherical flows: Model formulation and application. Submitted to *Theoretical and Computational Fluid Dynamics*. Preprint available at <https://ignite.byu.edu/publications.html> (2017)
19. Marusic, I., McKeon, B.J., Monkewitz, P.A., Nagib, H.M., Smits, A.J., Sreenivasan, K.R.: Wall-bounded turbulent flows at high Reynolds numbers: Recent advances and key issues. *Phys. Fluids* **22**(065103) (2010)
20. Medina M., J.A., Schmidt, H., Mauss, F., Jozefik, Z.: Constant volume n-Heptane autoignition using One-Dimensional Turbulence. *Combust. Flame* **190**, 388–401 (2018)
21. Meiselbach, F.: Application of ODT to turbulent flow problems. Ph.D. thesis, Brandenburgische Technische Universität Cottbus-Senftenberg (2015)
22. Monty, J., Stewart, J., Williams, R., Chong, M.: Large-scale features in turbulent pipe and channel flows. *J. Fluid Mech.* **589**, 147–156 (2007)
23. Moser, R., Kim, J., Mansour, N.: Direct Numerical Simulation of turbulent channel flow up to $Re_\tau = 590$. *Phys. Fluids* **11**(4), 943–945 (1999)
24. Papoulis, A., Pillai, S.U.: 4th edition edn. McGraw-Hill (2002)
25. Pope, S.: *Turbulent Flows*, 11th edn. Cambridge University Press (2011)

-
26. Schmidt, R.C., Kerstein, A., Wunsch, S., Nilsen, V.: Near-wall LES closure based on one-dimensional turbulence modeling. *J. Comput. Phys.* **186**, 317–355 (2003)
 27. Shiri, A.: Turbulence Measurements in a Natural Convection Boundary Layer and a Swirling Jet. Ph.D. thesis (2010)
 28. Sutherland, J., Punati, N., Kerstein, A.: A Unified Approach to the Various Formulations of the One-Dimensional-Turbulence Model. Tech. Rep. 100101, Institute for Clean and Secure Energy (ICSE) (2010)
 29. Wu, X., Moin, P.: A direct numerical simulation study on the mean velocity characteristics in turbulent pipe flow. *J. Fluid Mech.* **608**, 81–112 (2008)